Hydrogeology Journal (2021) 29:1885–1904
https://doi.org/10.1007/s10040-021-02354-8

PAPER

Multiple-tracers-aided surface-subsurface hydrological modeling for detailed characterization of regional catchment water dynamics in Kumamoto area, southern Japan

A. T. M. Sakiur Rahman[1] · Takahiro Hosono[2,3] · Yasuhiro Tawara[4] · Youichi Fukuoka[4] · Aurelien Hazart[4] · Jun Shimada[4]

Received: 23 July 2020 / Accepted: 26 April 2021 / Published online: 14 May 2021

Abstract

Integrated watershed modeling techniques have been applied in recent years to examine surface and subsurface interactions. Model performance is often evaluated by best fit of the hydrograph, which alone cannot explicitly explain whole catchment dynamics. To overcome this problem, this study incorporated multiple tracers (^{3}H, ^{85}Kr, and groundwater temperature) into a physically-based fully distributed modeling framework for characterizing regional-scale hydrological processes in Kumamoto, southern Japan. First, a simulation performed by a hydrometrically calibrated model showed satisfactory performance for river discharge and groundwater level. However, this model showed poor fitting for isotopic composition and temperature due to the structural uncertainty of the model. A new model was established reflecting recent deep bore log data and incorporating tracer data showed acceptable accuracy for hydrographs and tracers. Thus, more reliable estimates of groundwater storage, groundwater age and water flow paths were depicted over the regional catchment. Comparisons between the two models indicate that the model structure of an area with an uncertain lower boundary can be addressed by incorporating multiple tracer data. Tracer-aided models could be applied for a holistic understanding of contaminant transport dynamics besides flow simulation.

Keywords Integrated watershed modeling · Multiple tracers · Groundwater age · Regional scale · Japan

Introduction

Recent advances in simulating water transportation using physically-based process-oriented fully distributed models are deepening the understanding of hydrological processes by considering multiple water regimes (e.g., surface water, vadose zone water, groundwater) as an integrated system (e.g., Spanoudaki et al. 2009; Brunner and Simmons 2012; Barthel and Banzhaf 2016; Berg and Sudicky 2019). The fully coupled models can eliminate the interfaces between separate model modules and avoid problems related to theories and software packages for different water regimes (Brunner and Simmons 2012; Barthel and Banzhaf 2016). These approaches have been successfully applied over a wide range of watersheds to characterize: stream flow processes (e.g., VanderKwaak and Loague 2001; Frei et al. 2010; Weill et al. 2013); interaction between surface water and groundwater (e.g., Kollet and Maxwell 2006; Shen and Phanikumar 2010; Ala-aho et al. 2015; Chen et al. 2019; Boubacar et al. 2020); spatiotemporal distribution of contaminated sediments (Mori et al. 2015; Kitamura et al. 2016; Sakuma et al. 2017, 2018); rainfall responses to surface and subsurface flow systems (Li et al. 2008; Miles and Novakowski 2016); water and heat transport processes at the river–groundwater interface (Munz et al. 2017); groundwater residence time distributions (Kollet and Maxwell 2008; Maxwell et al. 2016; Jing et al. 2018;

✉ A. T. M. Sakiur Rahman
shakigeo@gmail.com

[1] Department of Earth and Environmental Science, Faculty of Science, Kumamoto University, 2-39-1 Kurokami, Kumamoto 860-8555, Japan

[2] Faculty of Advanced Science and Technology, Kumamoto University, 2-39-1 Kurokami, Kumamoto 860-8555, Japan

[3] International Research Organization for Advanced Science and Technology, Kumamoto University, 2-39-1 Kurokami, Kumamoto 860-8555, Japan

[4] Geosphere Environmental Technology Corporation, NCO Kanda, Awajicho Building 3F, 2-1 Kanda, Awajicho, Chiyoda-ku, Tokyo 101-0063, Japan

Wilusz et al. 2020); climate change impacts on hydrological processes (Goderniaux et al. 2009; Sudicky 2013; Davison et al. 2018; Erler et al. 2019); artificial recharge (Maples and Fogg 2019); coseismic hydrological changes (Hosono et al. 2019; Tawara et al. 2020); and hydrological cycles (Davison et al. 2018; Hwang et al. 2018; Chen et al. 2019).

Despite significant progress in integrated watershed modeling techniques (Berg and Sudicky 2019), there is an argument about the credibility of the models since, for the majority, model calibrations and validations relied solely on use of hydrographs (McDonnell and Beven 2014; McGuire and McDonnell 2015; Schilling et al. 2019). The hydrograph alone, however, cannot explicitly explore the whole catchment dynamics such as the origin of water, water ages, flow path, storage distribution, and solute transport (Birkel and Soulsby 2015; van Huijgevoort et al. 2016a). Incorporating tracer data is thus critically needed (McDonnell and Beven 2014; Birkel and Soulsby 2015; McGuire and McDonnell 2015; Knighton et al. 2017; Scheliga et al. 2019; Schilling et al. 2019) to build realistic models to explain catchment dynamics explicitly. For this reason, some recent studies (e.g., Fenicia et al. 2010; Birkel et al. 2010, 2011; Davies et al. 2011, 2013; Hrachowitz et al. 2013; Beven and Davies 2015) incorporated tracer data into rainfall-runoff models for characterizing sources of runoff, storage, water ages, and flow paths together with hydrometric data.

Although tracer-aided rainfall-runoff models represent a step towards an enhanced representation of the hydrologic cycle (Knighton et al. 2017; Schilling et al. 2019; Birkel et al. 2020), most of the tracer-aided models are lumped/semilumped conceptual models and applied in small catchments (Hrachowitz et al. 2013; McGuire and McDonnell 2015; Smith et al. 2016; Ala-aho et al. 2017; Birkel et al. 2020). For instance, Van Huijgevoort et al. (2016a, b) and Ala-aho et al. (2017) developed tracer-aided rainfall-runoff parsimonious models for simulating flux, storage, age, and mixing processes of waters in three small catchments (0.5–3.2 km^2) in Scotland, UK. Dehaspe et al. (2018) applied the same model for characterizing water and isotope transport processes in a small catchment (3.2 km^2) in Costa Rica. Kuppel et al. (2018) developed a fully distributed, physically-based ecohydrological model for characterizing water isotopes ($\delta^{18}O$ and $\delta^{2}H$) and age tracking across the hydro-pedological units in a small Scottish catchment (3.2 km^2). Piovano et al. (2019) characterized the runoff and water storage using a tracer-aided model in Granger Basin, Canada (7.8 km^2). Birkel et al. (2020) developed a semidistributed tracer-aided model for Howard River (126 km^2) catchment in Australia. However, their applications are still limited in hydrological modeling mainly due to a lack of long-term measured tracer data (McDonnell and Beven 2014; Birkel and Soulsby 2015) and model complexity in terms of parameterization and computational challenges (Dunn et al. 2010; McDonnell and Beven 2014; Birkel and Soulsby 2015, 2016; Schilling et al. 2019). In addition, an application of these models has not been expanded on a regional scale, although its development is important for conducting reasonable water management at this scale (Rassam et al. 2013; Barthel and Banzhaf 2016). Hence, incorporating multiple tracers into this type of model is a necessary task for better characterizing catchment water dynamics on a regional scale.

The main challenge for developing such a model is the collection of long-term tracer measurement data over a regional scale. The model domain of this study addresses regional groundwater flow systems in Kumamoto in the central part of Kyushu Island in southern Japan (Fig. 1); several studies (Taniguchi et al. 2003; Hosono et al. 2013, 2014, 2020; Hossain et al. 2016a, b; Zeng et al. 2016; Kagabu et al. 2017; Okumura et al. 2018) have characterized the groundwater age, flow dynamics, and biogeochemical processes using several tracers such as groundwater age tracers including sulfur hexafluoride (SF_6), tritium (^3H), chlorofluorocarbons (CFCs) and krypton (^{85}Kr), stable isotope ratios of water molecular (δD and $\delta^{18}O$), and aquifer temperature profiles. These studies demonstrated that the groundwater age tracers such as ^3H and ^{85}Kr concentrations are the most useful variables, while SF_6 and CFCs cannot be used for proper age determination due to contamination effects (Kagabu et al. 2017; Ide et al. 2020). In addition, δD and $\delta^{18}O$ do not show significant variations in time and space as former traces (^3H and ^{85}Kr) do due to small variations in altitude over the study area. Moreover, repeated measurement data of borehole temperature profiles were reported in this area (Taniguchi et al. 2003; Miyakoshi et al. 2020). An accumulation of these datasets provides an excellent opportunity to develop a multiple-tracers-aided model on a regional scale in Kumamoto, Japan.

The aim of this study was thus to develop a robust model for improving the understanding of catchment dynamics by bridging the physically-based process-oriented fully distributed model and multiple tracers (^3H, ^{85}Kr, and groundwater temperature) on a regional scale. The novel contribution of this study is to calibrate a model using multiple tracers together with hydrometric data for simulating the groundwater age. Before simulating groundwater age, the model structure was established through trial-and-error procedures for an area where delineation of the depth of the hydrogeological basement remains uncertain due to absence of impermeable stratum. Based on obtained simulation results, this study explicitly explains the catchment dynamics of the active groundwater flow systems of Kumamoto.

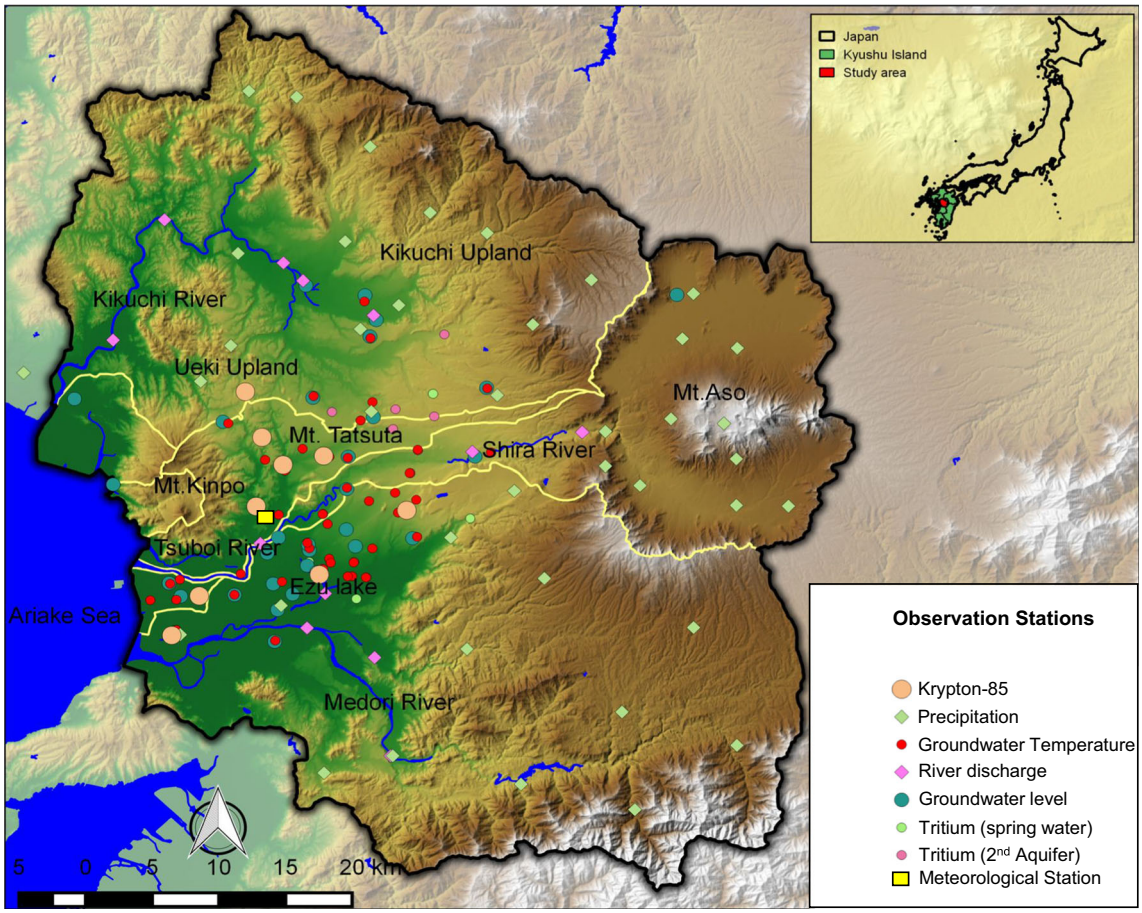

Fig. 1 Study area with locations of the meteorological station, precipitation gauge stations, groundwater monitoring wells, river discharge monitoring stations, sampling points for isotopic measurements, and groundwater temperature measuring wells

Study area, materials and methods

This study seamlessly simulated surface and subsurface flows, materials (^{3}H and ^{85}Kr) and heat transport, and groundwater age using GETFLOWS (General-purpose Terrestrial FLuidflOW Simulator) simulation code (e.g., Tosaka et al. 2000, 2010; Itoh et al. 2000; Mori et al. 2015; Tawara et al. 2020). Details of this simulation code (governing equations, verifications and validations) are provided in the Appendix and electronic supplementary material (ESM). The brief descriptions of the study area, prevailing climatic conditions, geological features, hydrogeological settings, data used for this study are presented in the following sections, while the steps followed for model development are explained in sections 'Numerical modeling' and 'Performance evaluation'.

Study area

The Kumamoto region is located in the central part of Kyushu Island in the southern part of Japan (Fig. 1). Geographically, the study area extends from 32°40′N to 33°N latitude and 130°30′E to131°05′E longitude, and it covers an area of about 2,689 km^2. Kumamoto is one of the largest groundwater utilization regions in Japan. About one million city dwellers depend entirely on groundwater resources for their domestic and drinking purposes (Oshima 2010; Shimada 2012; Taniguchi et al. 2019). Approximately 8×10^7 m^3 groundwater per year is withdrawn from 58 pump stations to meet the water demand (Hosono et al. 2013).

Topography and climate

The landscape of the study area is diverse and includes mountains, highlands, and lowland areas that are open to the Ariake Sea (Figs. 1 and 2a). The study area covers three major river basins, Kikuchi, Shira, and Midori River basins, along with other small watersheds. The area covers the Aso caldera volcanic mountains (1,592 m above mean sea level, amsl). There are three main highlands, Kikuchi, Takayubaru, and Ueki highlands (Fig. 1) which were formed during the last volcanic eruptions of Mt. Aso and have altitude ranging from 100 to 200 m (Miyamoto et al. 1962). The elevation becomes lower westwards in the plain area (elevation <8 m amsl) and towards the Ariake Sea (Fig. 2a).

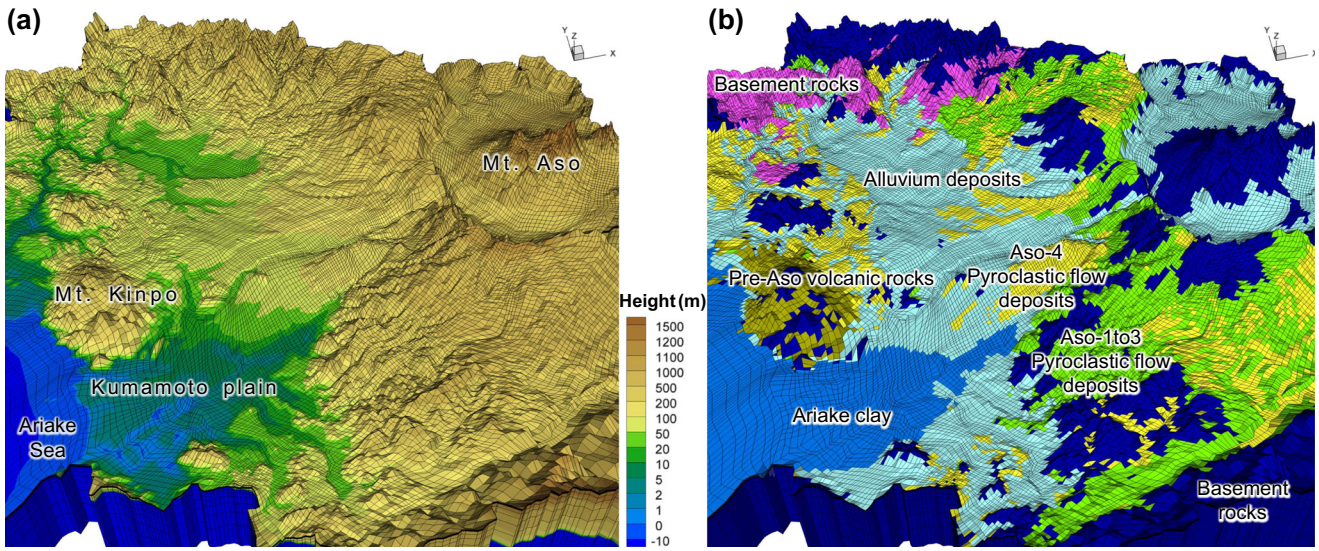

Fig. 2 Map showing 3D-model meshes with **a** digital elevation with 10 m resolution and **b** geological distribution of Kumamoto region (modified after Hosono et al. 2019)

The study area is characterized by a warm and humid climate. There are 40 precipitation gauge stations and one meteorological station within the area (Fig. 1). The average annual rainfall for the period of 1956–2007 varied between 1,723 mm (in the southeast) and 4,135 mm (in the northeast) with an average of 2,551 mm. Almost 40% of annual precipitation occurs during the rainy season (June and July), and precipitation is the main source of groundwater recharge in this area. The annual average temperature of Kumamoto meteorological station (Fig. 1) during the period of 1902 to 2017 ranged from 14.7 °C (recorded in 1917) to 18.2 °C (recorded in 1998) with an average of 16.1 °C. Further discussion on the climate of the study area can be found in Rahman et al. (2020a).

Geology

The geological units of the study area can broadly be divided into four groups (Hosono et al. 2020), the geological basement of Paleozoic metamorphic and metasedimentary rocks, Tertiary-Quaternary Pre-Aso volcanic rocks, the Quaternary Aso volcanic rocks (Ono and Watanabe 1985; Miyoshi et al. 2009), and alluvium deposits (Fig. 2b and Fig. S1 of the ESM). The Pre-Aso volcanic rocks are partially outcropped at the surface around the western foothill of Mt. Aso and at the Mts. Kinpo and Tatsuta. These volcanic rocks with older ages consist of major constituents of the hydrogeological basement (Fig. S1 of the ESM). The younger Aso volcanic rocks are distributed over the wide areas and composed mainly of flow lavas and pyroclastic flow deposits (Ono and Watanabe 1985), overlain by alluvium and the Ariake marine clays in the coast that are formed in the last transgression (Fig. 2b and Fig. S1 of the ESM). Aso volcanic rocks are subdivided into four units, based on the major volcanic eruption cycles, Aso-1, Aso-2, Aso-3, and Aso-4 from older to younger units (Ono and Watanabe 1985; Miyoshi et al. 2009). Of these, Aso-2 is a highly permeable formation as it consists of andesitic lava with joints and many porous structures (Hosono et al. 2013). There is impermeable lacustrine sediment, the Futa and Hanafusa layers, between the Aso-3 and Aso-4 (Fig. S1 of the ESM).

Hydrogeology

The aquifers in the study area are separated by the Futa and Hanafusa impermeable sediment layers into unconfined (named as the first aquifer) and semiconfined to confined aquifers (named as the second aquifer; Fig. S1 of the ESM; Taniguchi et al. 2003; Hosono et al. 2013, 2019, 2020; Rahman et al. 2020b). The first aquifer consists of unwelded Aso-4 pyroclastic deposits and alluvium sedimentary deposits, and the depth of this aquifer varies between a few meters to 90 m. The second aquifer is comprised of Aso-1 to Aso-3 pyroclastic flow deposits. The second aquifer is known as a deep aquifer, and its depth varies between 20 and 250 m. The groundwater in the study area is withdrawn mainly from the second aquifer. A detailed hydrogeological description is provided elsewhere (Hosono et al. 2013, 2019, 2020). There are two major groundwater flow lines, A–A′ and B–B′, which are further divided into four zones, recharge, mixed, discharge, and stagnant zones (Fig. S1 of the ESM) (Hosono et al. 2013, 2014). The cross-sectional views along these two major flow lines are shown in Fig. S1 of the ESM. The Kikuchi, Ueki, and Takayubaru highlands (Fig. 1) are the major groundwater recharge zones. Infiltration of precipitation is the primary source of groundwater recharge. In addition, groundwater recharge also occurs from rivers and the

artificial ponding of paddy fields near the mid-stream of the Shira River in groundwater recharge and mixed zones (Hosono et al. 2013; Taniguchi et al. 2019). In these areas, the soil infiltration capacity is very high (30–500 mm/day; Kiriyama and Ichikawa 2004; Takemori and Ichikawa 2007), and it accounts for almost one-third of the total groundwater recharge (Shimada 2012). In contrast, the majority of groundwater discharge occurs at the Ezu Lake in the plain area (Fig. 1 and Fig. S1 of the ESM).

Data source

The model generally requires areal property data such as surface and subsurface geology, meteorology, land use, and land cover. The seamless digital surface geological map of Japan (Geological Survey of Japan 2009) was used for mapping the surface geology (Fig. 2b). The digital elevation map (Fig. 2a) with a 10 m resolution reported by the Geographical Survey Institute of Japan was used for the modeling. Land use and land cover maps (Fig. S2 of the ESM) were used to estimate Manning's roughness coefficient (Table S2 of the ESM) provided by the Ministry of Land, Infrastructure, Transport, and Tourism (MLIT) of Japan and Land Surface Hydraulic Conductivity (LSHC) were also collected from MLIT (Table S2 of the ESM). The long-term (1957–2006) streamflow discharge data from 21 monitoring stations and groundwater level data (for the period of 1976–2006) from 43 monitoring stations (see Fig. 1 for their locations) were collected from MLIT database. The historical water use data such as river intake, paddy irrigation, and groundwater pumping were estimated by the Kumamoto City government for the same period. Precipitation and snow melt data (1956–2007) from 41 monitoring stations (Fig. 1) were collected from the Japan Meteorological Agency (2020) and the Ministry of Land, Infrastructure, Transport and Tourism (MLIT 2020) of Japan. A Thiessen polygon map was produced to show the distribution of precipitation in the area (Fig. S3 of the ESM). Potential evapotranspiration was estimated by the Thornthwaite method (Thornthwaite 1948) using the daily average temperature data of Kumamoto weather station from 1956 to 2007 considering the altitude effect on temperature by a factor of −0.0059 °C/m. A three-dimensional (3D) geological map of the study area (Fig. 2b) was prepared based on subsurface geological information from geological maps and borehole data reported in domestic reports. The hydraulic properties such as porosity and hydraulic conductivity were estimated from pumping test data reported in domestic reports. The multiphase flow properties such as intrinsic permeability, relative permeability, and capillary pressure were estimated from well test data, which are reported in the domestic reports. Further detail about the multiphase flow parameters for this study area can be found in Tawara et al. (2020).

There is a comprehensive temporal tracer data set for the study area; 47 vertical profiles of borehole groundwater temperature data were used (see Fig. 1 for their locations). Most of the stations have groundwater temperature records of very fine interval (1 m) from 1 to 221 m in depth repeatedly measured by previous researchers (Shimano et al. 1992 for records during 1986–1988; Taniguchi et al. 2003 for records during 2001; Uchida et al., Geological Survey of Japan, personal communication, 2017, for records during 2009–2010; and Ikawa et al., Geological Survey of Japan, personal communication, 2017, for records during 2011; Miyakoshi et al. 2020). This study also compiled historical ^{3}H concentration data from 26 measuring stations measured by the Water Resources Development Study Group (1975), Kumamoto Prefecture and Kumamoto City (1986, 1995) and Yamaguchi (2010). Kagabu et al. (2017) measured groundwater ^{85}Kr concentrations from nine wells that were used for validating the model derived during this study. Long-term (1940–2013) atmospheric ^{85}Kr and ^{3}H concentrations were also used, shown by Kagabu et al. (2017) as model input parameters.

Numerical modeling

GETFLOWS simulation code was used for fully coupled simulation of hydrological processes in Kumamoto region. GETFLOWS is a physically based, process-oriented fully distributed and multi-phase flow watershed modeling simulator (e.g., Tosaka et al. 2000; Mori et al. 2015). The GETFLOWS simulator has already been verified for several domains using analytical solutions, experimental study, and intercomparisons with other numerical codes (e.g., Tosaka et al. 1996, 2000; Itoh et al. 2000; Mori et al. 2015; Kitamura et al. 2016; Sakuma et al. 2017, 2018). Other (unpublished) verifications were also performed for simultaneous transport of heat and water for relevant cases, mainly for the subsurface domains. The details regarding verification and validation (V & V) of GETFLOWS are provided in the Appendix and ESM (Sections S2-S8 of the ESM). The procedures applied for developing the numerical models are presented in the following sections.

Model domain discretization

The integral finite difference method (IFDM) was applied for spatial discretization of the model domain in the GETFLOWS system (Mori et al. 2015). The computational fields were discretized into arbitrary deformed hexahedral grid blocks (Fig. 2) for adapting the geological heterogeneity, river networks and complex topography of this study area (Fig. 1). The surface model domain was discretized into 33,274 grids (Fig. 2) with horizontal resolution varying between 100 and 500 m, considering surface topographical and land-use features. Moreover, the grid block system was refined to match the

curvature and width of the main river channel. This ensures that no empirical parameters are necessary for connecting or disconnecting the watershed components like rivers, slope, subsurface soils, etc., and reduce the computational burden (Mori et al. 2015). The subsurface in the vertical direction was discretized into 28 layers with varying thicknesses; hence, the total number of analysis grids (998,220) was about one million.

Boundary conditions of the model

The no flow model boundary conditions were assigned at the borders in contact with land (Fig. 1) and at the bottom of the model that was set to 2,000 m below mean sea level. The active groundwater flows are assumed to be negligible below this depth. Furthermore, a zero-meter constant head boundary was assigned for the boundary between the model and the sea area (Ariake Sea; Fig. 1). The boundary of the model domain close to the seaside is approximately 20 km from the coastline and hence cannot inhibit groundwater and surface water flowing from the land into the sea. One of the main advantages of the GETFLOWS simulator for the fully coupled model is that it is not necessary to apply any a priori assumptions such as the first order exchange coefficient or interfacial boundary conditions which are mandatory for many existing simulators such as HydroGeoSphere (Therrien et al. 2010) and ParFlow (Kollet and Maxwell 2006). In other words, there is no need to assign boundary conditions for groundwater recharge and infiltration rates since this simulator can explicitly compute the interactions between air and water phases (Tosaka et al. 2000; Mori et al. 2015; Tawara et al. 2020). To enable the fully coupled simulation, two layers—an atmospheric layer and a surface layer—were placed over the subsurface layers ($K = 3, 4\ldots, 29, 30$) for coupling the fluid flows between surface and subsurface water regimes (Fig. S13 of the ESM). Constant atmospheric pressure and temperature were assigned as boundary conditions in the atmospheric layer, $K = 1$. Precipitation and potential evapotranspiration were assigned as boundary conditions in the surface layer, $K = 2$. A large value was given for the porosity and permeability for the uppermost layer ($K = 1$), whereas the effective porosity of the surface layer ($K = 2$) was set to 1.

For transport of materials (^{85}Kr and ^{3}H), similar boundaries (groundwater boundaries as stated above) were applied and the process was considered as simultaneous transport of water and materials. Furthermore, the material transport parameters diffusion coefficient and decay constant were used for simulating the behavior along the water flows (Table S5 of the ESM), while historical atmospheric concentrations of ^{87}Kr and ^{3}H in rainfall were assigned to the surface layer. In addition, the seamless simulation of groundwater and heat transport processes were considered following Domenico and Palciauskas (1973). Detailed description of the thermal boundary conditions is provided in the ESM (Section S8 of the ESM). In brief, the constant heat boundary condition (the long-term average temperature of Kumamoto meteorological station) was assigned to the surface layer of the model. The heat insulation boundaries were assigned at the borders in contact with land and the constant heat boundary (107 °C; Dong 2014) was set to the lower surface of the model. The initial geothermal gradient was set to 4.5 °C/100 m and the heat transport parameters such as heat capacity and thermal conductivity (Dong 2014) were treated as fixed values in this simulation. Dong (2014) did a field survey, and performed one-dimensional (1D), two-dimensional (2D) analytical solutions and 3D heat transport modeling to assess the specific heat and thermal conductivity values for different geological layers in Kumamoto region.

The model parameters, such as Manning's roughness coefficient (Table S1 of the ESM), land-surface hydraulic conductivity (Table S2 of the ESM), hydraulic conductivity and effective porosity (Table S3 of the ESM), thermal properties (Table S4 of the ESM), and material transport parameters (Table S5 of the ESM) are provided in the ESM.

Groundwater abstractions

There are a number of production wells (207) in the study area (Fig. S4 of the ESM). The historical daily groundwater abstraction data estimated by Kumamoto city government were used for modeling purposes. The GETFLOWS systems incorporate the well index approach proposed by Peaceman (1983) to address the impact of groundwater pumping in the model. The Peaceman well index approach is derived for single phase flows in anisotropic homogeneous ground and is applied to estimate groundwater production amount at a given pressure within a well shaft created in a coarse grid. This approach provides a good approximation for the grid with a production well, while the grid size is generally larger than the production well diameter and there is no mutual interference with the boundary conditions.

Model calibration and two different model settings

The model calibrations were performed following the trial-and-error procedures. The model performance was first assessed by comparing observed and simulated values of river discharges and groundwater levels. During the calibration process, the hydrogeological parameters of the aquifers (Table S3 of the ESM) were first adjusted within the range of values reported in the domestic borehole completion reports and previous relevant studies for this area (Shimada et al. 2012; Ichiyanagi et al. 2012; Hosono et al. 2019). It was confirmed that hydraulic conductivity is a fundamental parameter that has practical application, and other hydrogeological parameters, such as porosity, are not sensible for use in calibration in this study. Thus, an attempt was made to calibrate hydraulic

conductivity values for each unit and to check the performance of the model by assessing the fitting between simulated and observed river discharge and groundwater levels, as well as take account of multiple tracer data. These trial-and-error works were repeated until there was maximum fit between the calculation and observation results.

Through the aforementioned calibration, a model was first established following preexisting geological maps, assuming that each geological unit has each particular hydrogeological feature, and thus it was assumed that there is no active groundwater flow system in the Pre-Aso volcanic hydrogeological basement rocks beneath the second aquifer (Shimada et al. 2012; Ichiyanagi et al. 2012; Fig. S5a,c of the ESM). This model is called 'model-1'. Thereafter, another model called 'model-2' was established. Model-2 basically follows almost similar geological distributions and thus has hydrometric conditions similar to model-1. However, major changes were applied in model-2 with respect to its boundary condition of the bottom surface of the second aquifer, which was set to 100 m deeper than model-1 (Table S3 and Fig. S5b,d of the ESM). This model structure is based on the new results from a recent boring survey for deeper groundwater exploration (Nakayama et al. 2019). This recent survey confirmed the existence of the permeable layer in the upper part of the previously defined hydrogeological basement, i.e., Pre-Aso volcanic rocks. Nakayama et al. (2019) documented several groundwater production wells penetrating to a depth that is about 100 m into the Pre-Aso volcanic rocks and most of the production wells are continuously running for the purposes of groundwater abstraction. Hence, it clarified that there is a groundwater flow system in the upper part of the Pre-Aso volcanic rocks; Nakayama et al. (2019) called this the 'third aquifer', although the thickness of these deepest aquifers is not clearly defined from their field observations.

After performing calibrations with trial-and-error procedures, the hydraulic conductivity for the new aquifer unit was defined (Table S3 of the ESM), with properties similar to those obtained from model-1 for the aquifer units. In total, more than 100 variable sets were tested through a trial-and-error process used for constructing both models. Although the hydraulic conductivity values were generally similar for both models, the values for the second aquifer (Aso-1 to 3, pyroclastic flow deposit) in model-2 were slightly lower than the obtained values for model-1 (Table S3 of the ESM). For instance, the obtained hydraulic conductivity values for the second aquifer were between 1×10^{-5} and 1×10^{-0} cm/s for model-1 and these were between 1×10^{-5} and 2.5×10^{-1} cm/s for model-2. In addition, the adjusted hydraulic conductivity value for aquifer unit Togawa lava was slightly lower in model-2 than model-1 (Table S3 of the ESM). All calibrated values fall in the ranges of previous reports for the study area (Shimada et al. 2012; Ichiyanagi et al. 2012; Hosono et al. 2019).

For both models, steady-state simulations were performed to create the initial conditions representative of long-term (1976–2006) average groundwater levels, stream flow discharge, exchange flux and heat. Thereafter, daily time transient simulations for the validation period (2002–2006) were performed by both models using the daily meteorological data, tracer data and water use data.

Groundwater age simulation

Groundwater age simulation is often performed by particle tracking approaches and the 'age mass' concept. Particle tracking approaches generally consider only the advection motion of groundwater and ignore mixing and dispersion processes (Cordes and Kinzelbach 1992; Varni and Carrera 1998; Cornaton and Perrochet 2006). However, some studies have also documented that 3D backward particle tracking approaches (Weissmann et al. 2002; Zhang et al. 2018) with considerations of dispersion and mixing of groundwater provide reliable groundwater age in regional-scale aquifer systems. In this study, the mean groundwater age simulation was performed following the conceptual age mass concept (Goode 1996). The main governing equation for estimation of mean groundwater age (equivalent to mean transit time) is derived from the mass conservation principles and includes advection, dispersion, and mixing of water (Stolp et al. 2010; McCallum et al. 2015). Detailed methods are shown by Goode (1996). This approach can better infer the spatial distribution of mean groundwater age than by general particle tracking approaches (Cordes and Kinzelbach 1992; Varni and Carrera 1998; Cornaton and Perrochet 2006).

Performance evaluation

The river discharge simulation performance was evaluated using the Nash-Sutcliffe Efficiency (NSE) coefficient (Nash and Sutcliffe 1970), root mean square error (RMSE), and coefficient of determination (R^2). Simulated groundwater level was evaluated by RMSE, R^2, Pearson correlation coefficient (r) and relative interquartile range error (Q_{RE}). The Q_{RE} is effective for evaluating the time series amplitude of groundwater level. It can be expressed as (Sutanudjaja et al. 2011; Jing et al. 2018):

$$Q_{RE} = \frac{IQ^{md}_{7525} - IQ^{dt}_{7525}}{IQ^{dt}_{7525}} \quad (1)$$

where, IQ^{md}_{7525} is the interquartile range of calibrated groundwater level data and IQ^{dt}_{7525} is the interquartile range of observed groundwater level data.

Mean absolute error (MAE) and mean error (ME) were used to examine the tracer (^3H and ^{85}Kr) output results. Since relatively low numbers of measured tracer data are available, evaluations by the hydrograph-oriented matrix such

as NSE (Nash and Sutcliffe 1970) are less applicable (Ala-aho et al. 2017; Kuppel et al. 2018). However, this study could not estimate any goodness of fit statistics for the groundwater temperature simulation results, as the depth of the measured and simulated points were not coincident. Thus, the model performance for groundwater temperature simulation was assessed by visual inspection of the plots of measured and simulated groundwater temperatures in depth profiles.

Results

Steady-state simulation

A steady-state hydrological simulation was performed to create an initial condition for both model-1 and model-2. The steady-state simulation results for streamflow discharges and groundwater levels are shown in Fig. S6 of the ESM. The estimated NSE value for model-1 was 0.83, which indicates that the model performance is very good (Moriasi et al. 2007) with an RMSE of 2.57 (m^3/s). Model-1 also reproduced groundwater levels with a high correlation coefficient (r = 0.95; Fig. S21 of the ESM) and RMSE of 6.48 m over a wide range of groundwater levels, between 0.07 and 477.92 (m amsl). Groundwater temperature-depth profiles were also simulated at steady state using model-1 (Fig. 3 and Fig. S7 of the ESM), showing that the simulated temperature profile has a large gap in observations for most of the wells. In particular, the simulated groundwater temperature increases with increasing depth, which does not follow the measurement trends since the upper part of the Pre-Aso volcanic rock is considered as hydraulic basement rock (Shimada et al. 2012; Ichiyanagi et al. 2012). This finding clearly indicates that the aquifer in the area is much thicker than previously considered. Although the structure of model-1 does not represent the actual field conditions, it reproduced hydrographs with acceptable results. Several studies (e.g., McDonnell and Beven 2014; Birkel and Soulsby 2015; van Huijgevoort et al. 2016a) also confirmed that hydrograph fitting could not well-characterize catchment dynamics.

The groundwater temperature-depth profile was simulated for 47 wells, which are located over the study area. The simulations included groundwater recharge, major flow, discharge, and stagnant zones (Fig. S1 of the ESM). Visual inspection showed that the simulation results from model-2 exhibited better agreement with the observations than the results from model-1 for 30 wells, while the rest (12 wells, mainly located in the first aquifer) exhibited a close agreement for both models, and few of them showed better agreement with model-1 than model-2 (Fig. S7 of the ESM). Five wells showed a large discrepancy by both models. The results of steady-state hydrograph simulation by model-2 showed slightly higher errors than model-1 for streamflow discharges (Fig. S6 of the ESM). However, the simulated steady-state groundwater levels by model-2 showed lower errors than model-1. This result corresponds to some aspects, i.e. that the reproduction of hydrographs using tracer-aided models generally shows higher error than hydrometrically calibrated models (see review by Schilling et al. 2019).

The simulated groundwater level shows a wide range of spatial variation following the topography of the area for both models (Fig. 4a,b). The simulated groundwater level in the plain area was the same for both models, and means and maximums were different in the highland areas (= recharge areas): model-1 mean elevation 322.46 m amsl and model-2 mean elevation 321.91 m amsl, and model-1 maximum 1,548.73 m amsl and model-2 maximum 1,499.01 m amsl. Other fluxes such as groundwater recharge and

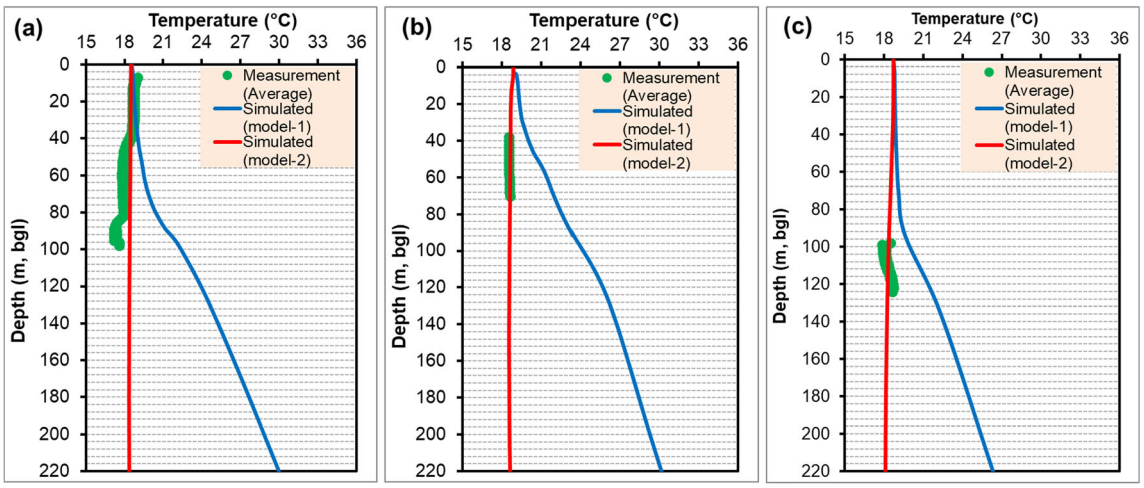

Fig. 3 Comparison between groundwater temperatures obtained from steady-state simulation and measured groundwater temperature data. The green dots represent average of measured data, while blue and red solid lines show results of model-1 and model-2, respectively. These three wells represent **a** shallow depth well, **b** medium depth well, and **c** deep well

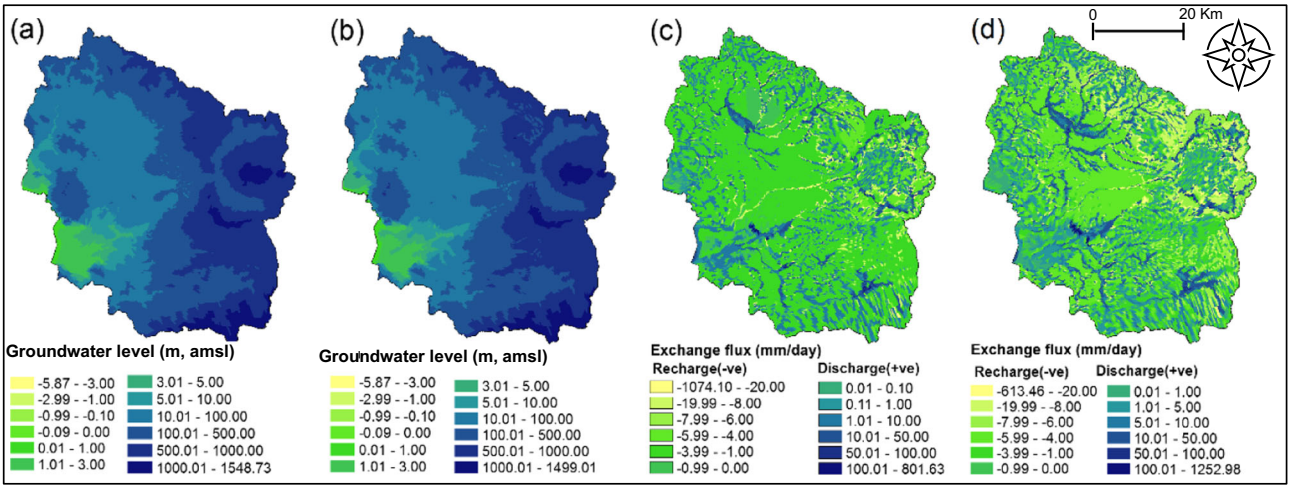

Fig. 4 Simulated scenario of steady-state models for **a**–**b** groundwater level and **c**–**d** water flux in terms of groundwater recharge and discharge. Model-1 simulation results (**a** and **c**), model-2 results (**b** and **d**)

discharge, also displayed some gaps (Fig. 4c,d). Figure S8 of the ESM exhibits a good agreement between observed and simulated (by model-2) recharge rates at some representative sites, with high r value (0.86), low AME (0.49 mm/day), and low ME (0.30). In addition, model-2 well captured the artificial recharge rates. Model-2 estimated a maximum groundwater recharge rate of 613.45 mm/day (Fig. 4), which is in good agreement with some observations (~500 mm/day; Kiriyama and Ichikawa 2004; Takemori and Ichikawa 2007). However, model-1 estimated the maximum groundwater recharge rate of 1,074.10 mm/day, possibly due to overestimation of groundwater recharge, and thus the estimated groundwater residence time is faster than in the actual field conditions. Figure 4c,d shows that subsurface water discharge occurs along the major rivers and in lake areas, which was expected, and hence deemed an adequate inference for this model.

Transient simulation

Transient-state simulations were carried out by both models for 5 years (2002–2006) and reproduced daily streamflow discharges, groundwater levels, and tracer concentrations (^{3}H and ^{85}Kr). The simulation was performed for 21 river stations. Figure 5 shows results for streamflow discharges at three representative stations. As shown in Fig. 5, there is a good agreement between the observed and simulated discharge data for both models. For model-1, the NSE values obtained from the comparison between observation and simulation varied from 0.46 (Dai Roku Hashi station) to 0.90 (Chukobashi station; Table S6 of the ESM) with an average value of 0.70, and R^2 ranged between 0.59 and 0.92 with an average value of 0.80. The performance of model-2 showed that the average NSE value for seven stations was 0.71, with an R^2 value of 0.79 (Table S6 of the ESM). The data at Dai Roku Hashi also showed a comparatively large discrepancy between observation and simulation compared to other stations.

Some examples of transient simulation of groundwater levels are shown in Fig. 6. Instead of plotting the actual groundwater levels, Fig. 6 shows the anomalies of observed and simulated groundwater level data related to their long-term mean values for analyzing the discrepancy between model results and observations. The model performance was evaluated by the Pearson correlation coefficient (r), which indicates the timing/punctuality, and relative inter-quartile range $|Q_{RE}|$, which measures the magnitude of amplitude error (Sutanudjaja et al. 2011; Jing et al. 2018). Models that simulated groundwater level showed a good agreement with observed data. The r and $|Q_{RE}|$ values for the well in Gotsu (Fig. 6a) were 0.84 and 11.60% for model-1 and 0.78 and 0.99% for model-2, respectively. The mean and median values of model results and observation data are also shown in Fig. 6. The r value for model-1 is higher than that of model-2; however, $|Q_{RE}|$ for model-2 is lower than that of model-1. Moreover, the estimated mean and median values of model-2 were closer to the observed values than the results of model-1. Similar results were also obtained for the well located in Izumi (Fig. 6b); however, the opposite results were found for the well in Koshi (Fig. 6c).

The simulation was examined using 43 groundwater monitoring stations. The estimated r value between observation and simulation data for model-1 (42 stations; one station has no good observation records) was 0.96 for the period during 2002–2006, while it was 0.94 for model-2 for the same period (Fig. S9 of the ESM). Moreover, the r

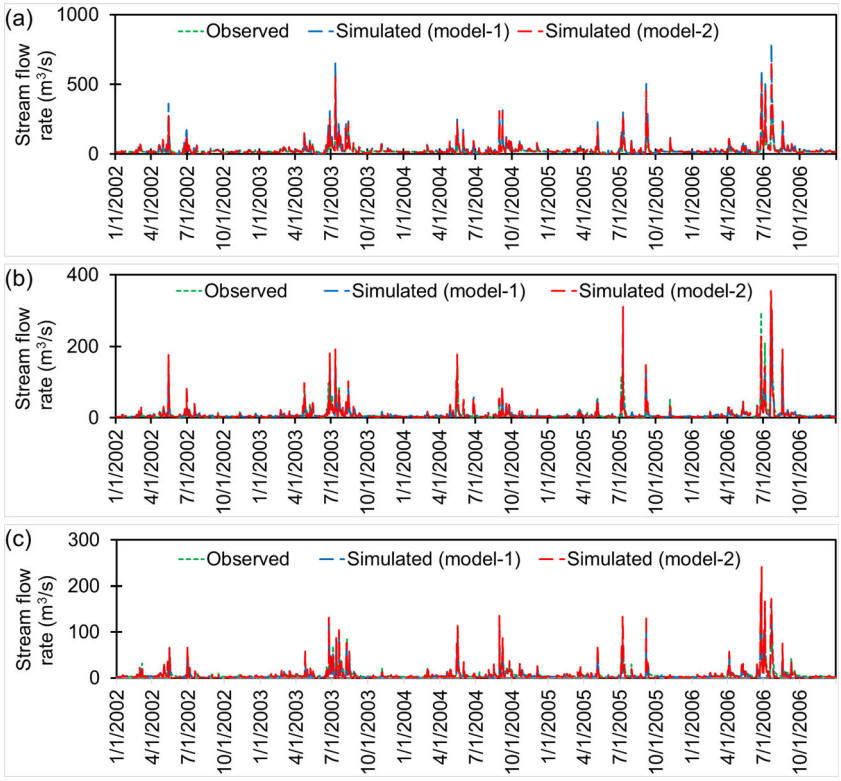

Fig. 5 Comparison between observed and model simulated results for stream flow discharge for stations located in three major river basins in the study area: **a** Jinnai station in Shira river basin, **b** Hirose station in Kikuchi river basin, **c** Mifune station in Midori river basin

values calculated between the median of observed and simulated were 0.96 and 0.94 for model-1 and model-2, respectively. This study also examined the seasonal responses of the model results (Fig. S10 of the ESM). These assessments generally show identical patterns that indicate that the model results do not exhibit any bias to a particular season. It may be noticeable that the error for the summer season, when most of the precipitation occurs, is the highest for model-1, while it is the lowest for model-2. Despite some discrepancies between observed and

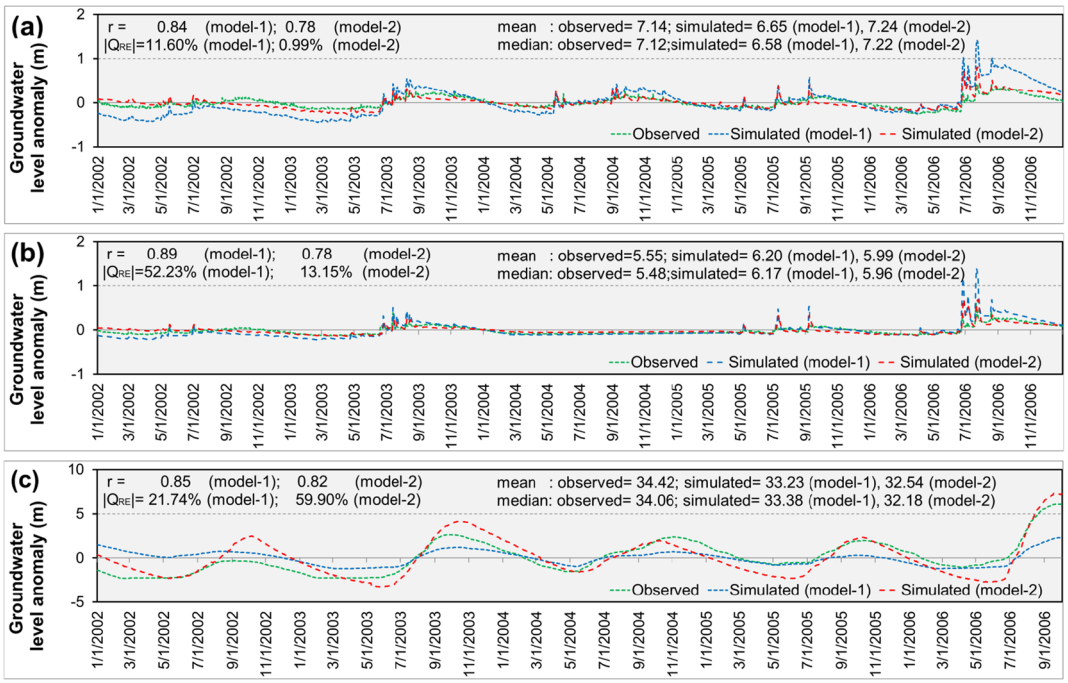

Fig. 6 Comparison between the observed and simulated groundwater level anomaly of three groundwater observation stations: **a** Gotsu shi, **b** Izumi, and **c** Koshi

simulated data, model results generally well captured the seasonal groundwater dynamics.

Tracer simulation

Simulation was performed to reproduce ^{3}H and ^{85}Kr concentrations in groundwater for all the grids of the model domain. The ^{3}H time series for 23 wells and 3 springs over the study area were used to evaluate the simulation performance of the models. Note that, tracers like ^{3}H and ^{85}Kr have no continuous measured records. For ^{3}H, stations with at least 2 years of measured records during the period of 1957–2010 were used to validate the results obtained from the models. Figure 7 displays typical examples of comparisons between measured data and model results. Figure 7a shows groundwater data from the plain area, whereas Fig. 7b,c display groundwater data from Aso Mountain and spring water from Ezu Lake, respectively. The simulation results from model-2 seem to exhibit a good correspondence with measured data for all three stations. Plots for all stations are shown in Fig. S11 of the ESM. The estimated MAE and ME were 10.63 and 6.36 TU, respectively, for model-1 and the difference in mean between measured (5.88 TU) and simulated data (12.24 TU) was very high (6.36 TU) for model-1. On the other hand, model-2 reproduced ^{3}H concentrations with reasonable accuracy, with MAE of 5.71 TU, ME of −0.27 TU and a small difference in mean between simulated and measured data of 0.28 TU. Thus, the discrepancy between measured data and simulation results is far smaller in model-2 than model-1.

Similarly, ^{85}Kr concentration data of nine stations were compared to the simulation results for both models (Fig. 8 and Fig. S12 of the ESM). Model-1 exhibited an unsatisfactory performance for ^{85}Kr concentration simulations for all stations since the difference between measured and simulated were very high. On the other hand, model-2 reasonably reproduced the ^{85}Kr concentrations for almost all the measuring stations except a station located in Ippongi. There are some stations where measured ^{85}Kr concentrations were nil as these are located in the stagnant zones, and model-2 results showed almost zero for these stations. The notable improvement in the performance of ^{85}Kr simulation results from model-2 is consistent with results from the steady-state simulation of groundwater temperature.

Discussion

Applicability of multiple-tracers-aided hydrological modeling

Development of the two models and recent deep bore log data provide an opportunity to test the applicability of the multiple-tracer-aided model for reducing structural uncertainty. The findings of this study clearly demonstrate that hydrograph fitting alone could not determine the groundwater storage in an area where lower surface boundary conditions remained uncertain. Hence, the classical modeling approaches are not suitable for this type of aquifer system. The uncertainty of the model structure can be addressed in the model by incorporating tracer data. Reproduction of tracer data along with hydrograph fittings can increase the credibility of the model and reflect reliable subsurface conditions such as depth of the bedrock and groundwater storage. These factors have a significant influence on the estimation of groundwater residence time which is very useful in understanding contaminant transport dynamics (Ameli et al. 2016; Heidbuchel et al. 2013; Kim et al. 2016, Basu et al. 2012). Some studies have determined that tracer data can be used to improve the conceptualization of models as well as examine their internal consistency when tested at local scale (Tsuboyama et al. 1994; Dunn et al. 2010; Delavau et al. 2017; Schilling et al. 2019). The results reported here demonstrate that the methodology can be extended to a study at regional scale.

Regional catchment water dynamics in Kumamoto

As mentioned in the previous section, the updated model (model-2) provides better visualization of the subsurface systems such as groundwater storage and depth of the bedrocks

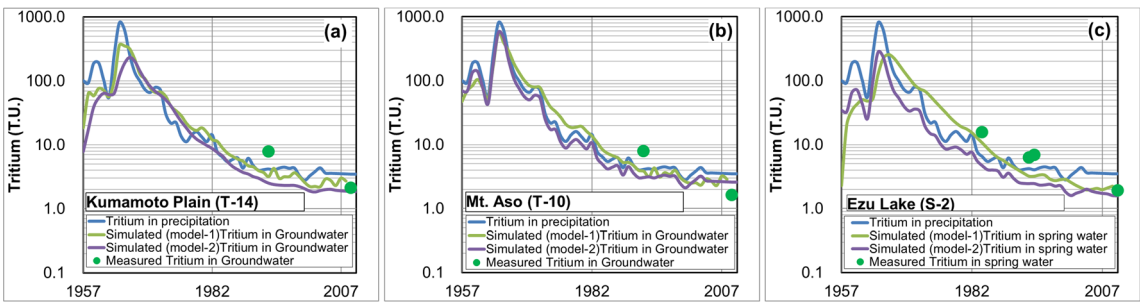

Fig. 7 The ^{3}H concentration time series at different locations in the study area. ^{3}H in precipitation is indicated by the blue line. Measured ^{3}H values in groundwater are shown by green plots and simulated time series of ^{3}H in groundwater for model-1 and model-2 are shown by light green and purple lines, respectively

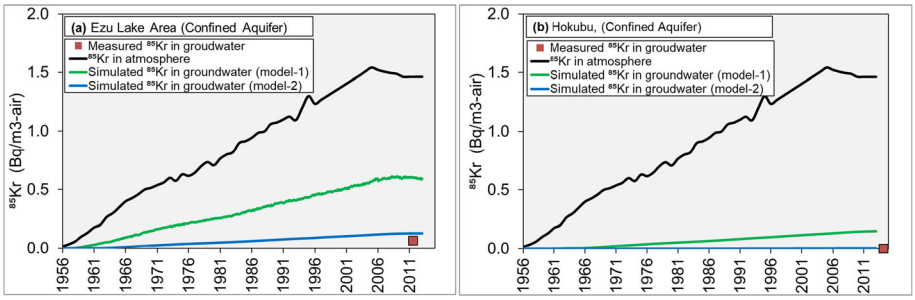

Fig. 8 The ^{85}Kr concentrations time series in the atmosphere and groundwater. Black line, red square, green and blue lines indicate ^{85}Kr values in the atmosphere, measured ^{85}Kr in groundwater, and simulated (model-1 and model-2) ^{85}Kr in groundwaters, respectively. The wells are in the **a** discharge area and **b** stagnant area. Note that measured ^{85}Kr concentration was below the detection limit (0.0015 Bq) for the site illustrated in part **b**

of the Kumamoto region. Therefore, model-2 was used for flow paths and mean groundwater age simulation. Figure 9a displays the 3D simulated orthogonal projection of surface and subsurface coupled streamlines by model-2. The yellow

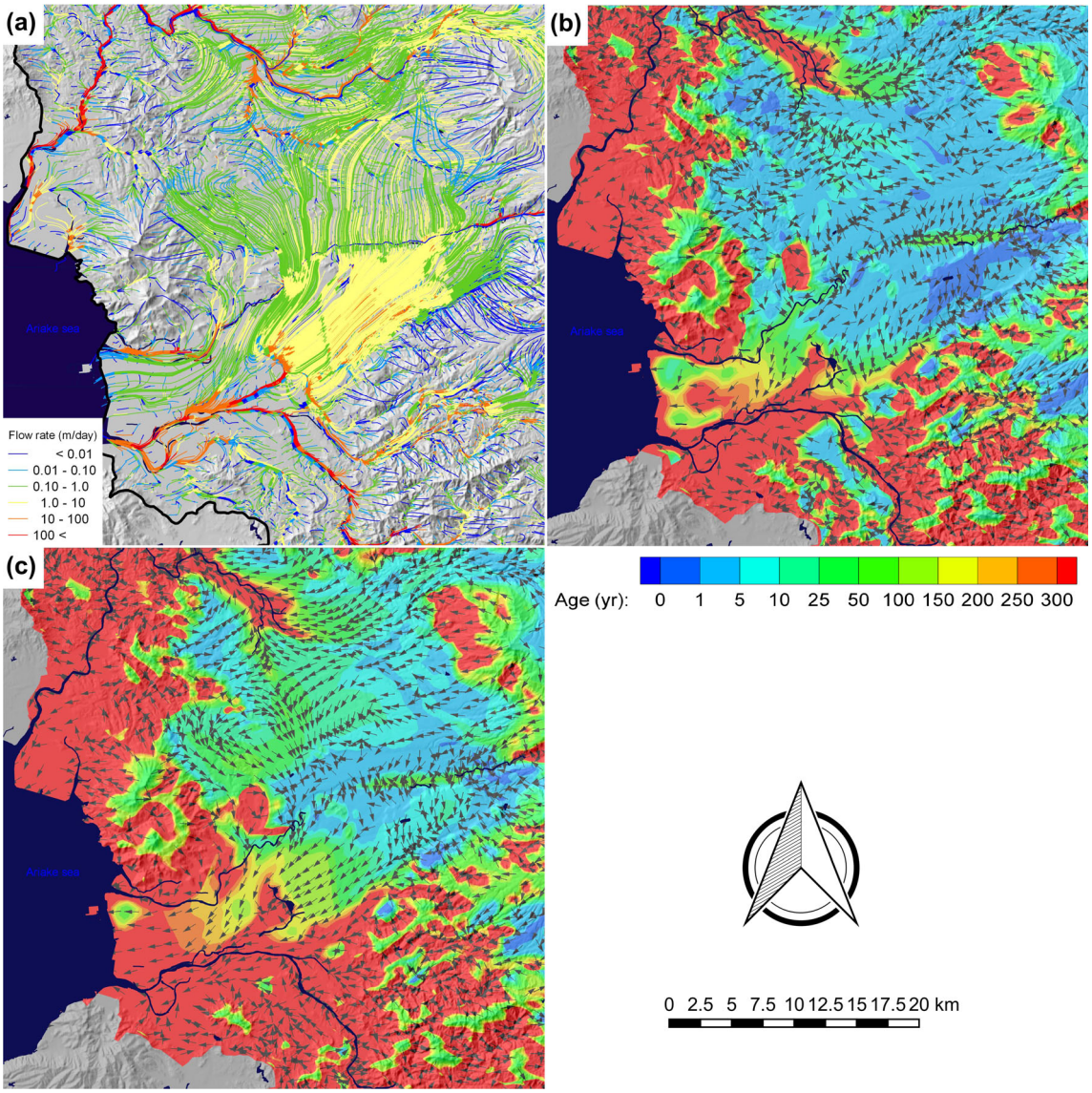

Fig. 9 Spatial distributions of simulated **a** surface and subsurface coupled streamlines in equilibrium state with velocity of water flow, **b** groundwater age in the first and **c** second aquifers with water flow directions as shown by small gray arrows

lines display relatively faster (1.0–10 m/day) groundwater flow than other part of aquifers (e.g., green line, 0.1–1.0 m/day) in the study area, where active groundwater flows are facilitated by the high infiltration features in and around the midsection of the Shira River and the presence of highly porous formations of Togawa lava. The red lines represent the rapid flow of streams or surface runoff with higher velocities.

Model-2 was also used for simulating the mean groundwater age distribution following the age mass concept, which includes advection, diffusion, and mixing of waters (Goode 1996). The solution of the equations yields mean groundwater ages ranging from a few years to 300 years in the first (unconfined) aquifer in the study area (Fig. 9b). As expected, the groundwater is generally older in the southwestern part near the coastal area in the stagnant zone, and younger waters are found in the recharge areas. Groundwater ages were also visualized for the second (confined) aquifer that showed older ages compared to the unconfined aquifer but shows similar spatial patterns (Fig. 9c). The simulated mean groundwater ages match well with the findings of earlier studies (Momoshima et al. 2011; Kagabu et al. 2017), while they were considered only for point data along two major flow lines (Fig. S1 of the ESM). For example, Kagabu et al. (2017) estimated groundwater age and found young (approximately 16 years) waters in the recharge area (A–A′ flow line), and the simulated groundwater ages for the same locations were within the same range (10–25 years). Although the estimated groundwater age along the B–B′ flow line (>55 years) was not defined precisely due to limitations of the ^{85}Kr age tracer method (Kagabu et al. 2017), the simulation can determine that the groundwater ages range from ca. 10 to 100 years, except in the plain to coast areas where older aged (mostly >250 years) groundwater is found (Fig. 9c). The results from model-2 showed a more precise and accurate view of water flow pathways and time ranges than those from model-1 or any other studies from point observation datasets at regional scale.

Limitations and implications

Tracer simulation results for some measuring stations (Figs. S7, S11 and S12 of the ESM) still showed large errors, and some of them are found in the same areas. Hence, these discrepancies are mainly related to the local heterogeneities. Some sources of errors might be related to grid (Bathurst 1986; Hardy et al. 1999) and DEM resolutions (Ivanov et al. 2004; Zhang et al. 2016)—for example, this study used similar grid size (100–500 m resolution) to other reported studies, but DEM resolution (10 m) was coarser than those used in some previous works (e.g., van Huijgevoort et al. 2016a) with high-resolution DEM (1 m) and grid (100 × 100 m), mainly because this study treated larger areas than previously tested.

Table 1 The parameters used in the governing equations for operation of the GETFLOWS

Categories	Required parameters	Unit	Notation
1. Meteorology	Precipitation	(mm/day)	P
	Air temperature	(°C)	T_a
	Wind velocity	(m/s)	U
	Hours of sunlight	(hr)	N
	Relative humidity	(%)	RH
	Amount of solar radiation	(W/m^2)	S_a
2. Land surface processes	Elevation	(m)	ξ
	Manning's roughness coefficient	(m$^{-1/3}$ s)	n
	Albedo	(−)	A
	Bulk transfer coefficient	(−)	C_H
3. Subsurface fluid flow	Intrinsic permeability	(m^2)	K
	Effective porosity	(−)	ϕ
	Relative permeability	(−)	k_r
	Capillary pressure	(Pa)	P_c
4. Dissolved materials transport	Soil/rock density	(kg/m^3)	ρ_s
	Molecular diffusion coefficient	(m^2/s)	D
	Tortuosity factor	(−)	τ
	Dispersion length	(m)	α_L, α_T
	Decay constant	(1/s)	λ
5. Heat transport	Heat capacity	(J/kg/K)	c_r
	Thermal conductivity	(W/m/K)	κ

Model performance for simulating tracers (point data) and hydrographs may increase using subgrid parameterization techniques (Samaniego et al. 2010; Decker 2015) and high-resolution DEM (Beven 1989; Smith et al. 2004; Ivanov et al. 2004; Zhang et al. 2016). In turn, if the numbers of grids increase and the complexity of the model increase, it takes more time for processing and calculations, which must simultaneously be improved for more practical application and for general users. [It took ca. 1–2 days to run a set of simulations for the case of the present study, while parallel computation was run by more than 100 computers with multicore processors (Intel(R) Core(TM) i7-3960X CPU @ 3.30 GHz).]

Although there are some limitations and scope for further improving the modeling, the obtained results and relevant studies (e.g., Knighton et al. 2017; Schilling et al. 2019; Birkel et al. 2020) showed that tracer incorporation is fundamental in increasing the reliability of the model. Although multiple tracer data like those shown in this study (^{3}H and ^{85}Kr concentrations and temperature log data) are not often available in many regions of the world, some general hydrochemistry data or dissolved contaminants data may be commonly available globally. For instance, some recent studies have started involving dissolved nitrate ions in modeling to understand transportation and behavior of nitrogen contamination once loaded on the ground surface and subsequently carried with water flows in aquifers with transformation (e.g., Almasri and Kaluarachchi 2007; Matiatos et al. 2019); nitrogen concentration data are widespread in time and space. Here it is suggested that such work can also be used for validating the structure of models designed to explain both water flows and tracer concentrations by comparing simulated and observed values. Thus, it must be important to seek some other tracers that are ubiquitous and applicable for developing reliable models more globally in the future.

Conclusions

This study presents the results of two different models calibrated using an integrated watershed modeling approach for the Kumamoto region (Japan) with diverse geomorphological settings. The model results were evaluated both for the steady-state and transient simulations. The model calibrated using hydrometric data generally exhibited a good performance for streamflow hydrographs and groundwater levels. However, hydrograph fitting could not determine the actual groundwater storage, which can be confirmed by incorporating multiple tracer data. The updated model (model-2) with deeper hydrogeological boundary conditions successfully reproduced multiple-tracer movement (^{3}H, ^{85}Kr, and temperature) as well as hydrographs with an acceptable error. This model can provide a better explanation for catchment water dynamics in Kumamoto at regional scale. The findings of this study will provide useful information for water resources managers when attempting to understand surface and subsurface hydrological processes and when characterizing sources, distribution, and transport processes of contaminants. Furthermore, this study ensures that multiple-tracer inclusion in the model can reduce the structural uncertainty of the model for an area where the lower boundary of the aquifer is uncertain. The obtained results represent the first step in understanding detailed catchment dynamics at a regional scale using an integrated watershed modeling technique incorporating multiple tracer data. The findings of this study encourage further studies using tracer data together with hydrometric data for detailed characterization of surface–subsurface hydrological processes.

Appendix 1: governing equations of GETFLOWS

The governing equations of GETFLOWS simulator include fluid flow, transport of dissolved materials (e.g., concentrations and isotope ratios), and heat. Fluid flow is modeled as coupled surface and subsurface flows, and the associated conjunctive behavior of the dissolved materials and heat can be traced simultaneously. The individual governing equations are based on the mass and energy conservation laws. Table 1 summarizes the major parameters shown in the governing equations.

Coupled surface and subsurface fluid flows

The governing equations are derived from the mass conservation laws for each fluid phase (surface and subsurface). Manning's law was adapted for surface water flow, and diffusive wave approximation of Saint Venant equations was applied to estimate the surface water velocity in 2D space. Subsurface fluid flows (i.e., groundwater) are characterized by generalized Darcy's law in 3D space. The law of mass conservation for both surface and subsurface fluid flows can be expressed as follows:

$$-\nabla \cdot M_p + \rho_p q_p = \frac{\partial\left(\phi \rho_p S_p\right)}{\partial t}, (p = \text{water}, \text{air}) \quad (2)$$

where, ∇ and ρ_p denote differential operator and density (kg/m^3) of fluid, respectively. Mass flux of fluid (kg/m^2/s) and

volumetric flux of source and sink ($m^3/m^3/s$) are represented by M_p and ϕ, and q_p and t represent effective porosity (m^3/m^3) and time (s), respectively. The saturation of fluid (m^3/m^3) is embodied by S_p, and the subscript p is used to denote the air (a) or water (w) phase of the fluid. The effective porosity value is 1.0 in Eq. (1) for the surface fluid.

Fluid mass flux (M_p) per unit area can be given by adapting Manning's law for surface flow and Darcy's law for subsurface as follows:

Surface fluid:

Water

$$M_p = -\frac{\rho_p R^{\frac{2}{3}}}{n_l} \times \sqrt{\left|\frac{\partial h}{\partial l} + \frac{\partial z}{\partial l}\right|}\,\mathrm{sgn}\left(\frac{\partial h}{\partial l} + \frac{\partial z}{\partial l}\right), (p = \text{water } l = x, y) \quad (3)$$

Air

$$M_p = -\frac{\rho_p K k_{r,p}}{\mu_p}\nabla\left(P_p + \rho_p g z\right), (p = \text{air}) \quad (4)$$

Subsurface fluid:

$$M_p = -\frac{\rho_p K k_{r,p}}{\mu_p}\nabla\left(P_p + \rho_p g z\right), (p = \text{water, air}) \quad (5)$$

where, n_l indicates Manning's roughness coefficient ($m^{-1/3}$ s). The R, h and l represent hydraulic radius (m), surface water depth (m), and surface water flow distance (m), respectively. The z, g, μ_p and P_p denote elevation from datum surface (m), gravitational acceleration (m/s^2), viscosity coefficient (Pa s), and pressure (Pa), respectively. K and $k_{r,\,p}$ are intrinsic permeability (m^2) and relative permeability, respectively.

The surface-water depth h was computed from the water saturation and the height of the grid block in the surface environment. The difference between air and water pressure is associated with capillary pressure P_c (Pa):

$$P_a = P_w + P_c \quad (6)$$

The relative permeability and capillary pressure are a function of the water saturation in the two-phase flow system. Additionally, the fluid density and viscosity coefficient are a function of fluid pressure and temperature. The total of fluid saturations is treated as 1.0 in the two-phase flow system as follows:

$$S_w + S_a = 1.0 \quad (7)$$

Transport of dissolved materials in water

This study coupled the water flow with mass transport of groundwater age tracers (^3H and ^{85}Kr) as dissolved materials in water. The mass balance of dissolved material i in water can be expressed as the following advection-diffusion/dispersion equation considering radioactive decay as:

$$-\nabla\cdot\left(M_w C_{w,i}\right) + \nabla\cdot D_{w,i}\nabla\left(\rho_w C_{w,i}\right) + \rho_w q_w C_{w,i} - \phi\lambda_i C_{w,i} = \frac{\partial\left(\phi\rho_w S_w C_{w,i}\right)}{\partial t} \quad (8)$$

where, $C_{w,\,i}$ is the mass fraction of dissolved material i in water (kg/kg) (defined as the mass of dissolved material i per unit mass of water in each grid). $D_{w,\,i}$ and λ_i are the hydrodynamic dispersion coefficient (m^2/s) and the decay constant (1/s) of dissolved material i, respectively. The hydrodynamic dispersion coefficient $D_{w,\,i}$ is computed from the molecular diffusion coefficient, tortuosity factor, dispersion length, and effective water velocity in porous media. The $\lambda_i$is derived from the half-life of each radioactive material (^3H and ^{85}Kr). Adsorption and desorption are not considered for these isotopes. The molecular diffusion coefficient is considered as a constant value in this study.

Heat transport

The governing equation for heat transport modeling consists of energy conservation equations for fluid and solid phases in addition to mass balance equations for air and water phases under nonisothermal conditions. The equation can be expressed as:

$$-\nabla\cdot(M_w H_w) - \nabla\cdot(M_a H_a) + \nabla\cdot\kappa_f\nabla T + \nabla\cdot\kappa_s\nabla T + \rho_w q_w H_w + \rho_a q_a H_a + E_s = \frac{\partial(\phi\rho_w S_w U_w + \phi\rho_a S_a U_a + (1-\phi)\rho_s U_s)}{\partial t} \quad (9)$$

where, H_w and $H_a$are the enthalpies of water and air phases (J/kg), respectively, κ_f and κ_s are the saturation weighted average thermal conductivities of fluid and solid phases (W/m/K), respectively, T is the average temperature for both fluid and solid phases (K), E_s is the volumetric heat flux of the sink and source in the solid phase ($J/m^3/s$), ρ_s is the density of solid phase (kg/m^3), and U_w, U_a and U_R are the internal energies of water, air, and solid phases (J/kg), respectively. The heat transport parameters such as heat capacity and thermal conductivity are treated as fixed values in this simulation.

Appendix 2: verification and validation

In the early stage of the development of the GETFLOWS simulator, Tosaka et al. (2000) verified surface flow simulation by comparing with experimental results, and its application was proved in some local fields (Itoh et al. 2000). Studies (Tosaka et al. 1996, 2000) also compared results of some analytical solutions for surface–subsurface flow coupling simulation, e.g., relative permeability and capillary rise of water, using GETFLOWS (Tosaka et al. 1996, 2000). More recently, Mori et al. (2015) have shown inter-comparisons with another simulator (i.e., InHM, VanderKwaak 1999) for surface flow and sediment discharges. The detailed verification and validation (V & V) of GETFLOWS are available through the website of the Geosphere Environmental Technology Corp. (2020) or direct email. However, some basic information on V & V procedures and model discretization are provided also in this paper's Appendices and ESM, since these manuals are not completely accessible through their website.

In the development of the GETFLOWS systems, a lot of verification was undertaken for relevant cases, mainly for the subsurface domain, by comparing results of analytical solutions, inter-comparisons with other simulators, and using results of experimental study. Detailed descriptions of the analytical solutions are provided in Sections S3–S8 of the ESM. Briefly, an analytical solution for the conceptual model is shown in Fig. S14 of the ESM and numerical simulation for 1D saturated horizontal groundwater flows (Fig. S15 of the ESM) and 2D vertical flows (Fig. S16 of the ESM) are described in Section S3 of the ESM. Details of the numerical model and analytical solutions are provided in Tables S7–S10 of the ESM, and their results are presented in Tables S11 and S12 of the ESM. Similarly, the simulator was also verified using experimental results of a falling head test to monitor water level changes over a given time (Tosaka 2007; Section S4, Figs. S17–S19 and Tables S13–S15 of the ESM). Furthermore, verifications for the pumping test of a confined aquifer (Figs. S20–S22, Tables S16–S18 of the ESM) and capillary pressure of unsaturated zone (Figs. S23 and S24, Tables S19–S21 of the ESM) were provided in sections S5 and S6. These comparisons showed excellent agreement between analytical and numerical solutions and ensured that there is no bug in the GETFLOWS numerical code for water flow simulation.

Comparison of simulation results between GETFLOWS and TOUGH2 (Pruess et al. 1999), another multiphase flow simulator, is documented in Section S7 of the ESM, for simulating groundwater flows in porous media with heterogenous permeability (Fig. S25 of the ESM). This inter-comparison example was taken from the international HYDROCOIN project for groundwater flow simulation evaluation (Thunvik 1987). A 2D heterogeneous porous medium placed between impermeable layers was considered for the simulation (Fig. S26 of the ESM). Initially, the system was kept in an unsaturated condition; then, water was injected to allow fluids flow through the media replacing the air (Fig. S26 of the ESM). Further details on model domains and properties are given in Tables S22–S24 of the ESM. Comparisons of transient simulation results between GETFLOWS and TOUGH2 (Fig. S27, Fig. S28 of the ESM) showed almost identical results over the time steps. Overall, the GETFLOWS simulations showed an excellent agreement with TOUGH2 for transient simulation (Fig. S27, Fig. S28 and Table S25 of the ESM).

Several previous studies have already demonstrated the capability of GETFLOWS for simultaneous simulations of water flows, isotope tracers and sediment transport (e.g., Mori et al. 2015; Kitamura et al. 2016; Sakuma et al. 2017, 2018; Hosono et al. 2019; Tawara et al. 2020). However, number of studies simulating for heat transport processes along with groundwater flow systems are still small on certain field sites using GETFLOWS. In principal, performance of GETFLOWS simulation is verified with the theoretical solutions (Domenico and Palciauskas 1973) for simultaneous transport of groundwater and heat. All the model parameters (Table S26) relevant to the Domenico and Palciauskas 1973) problem (Fig. S28 of the ESM) and numerical simulation details are provided in Section S8 of the ESM. All numerical simulation results extracted both for vertical and horizontal plains, and the comparisons between analytical and numerical solutions, showed identical results (Fig. S30 of the ESM). Hence, GETFLOWS is capable of simulating heat transport processes.

Supplementary Information The online version contains supplementary material available at https://doi.org/10.1007/s10040-021-02354-8.

Acknowledgments A.T.M.S.R. wishes to thank members of hydrology laboratory in Kumamoto University and staffs in Geosphere Environmental Technology Corporation for their permanent supports and fruitful discussion during the study.

Funding information A.T.M.S.R. was supported by MEXT scholarship, Japan. T.H. was supported by the JSPS Grant-in-Aid for Scientific Research B (17H01861).

References

Ala-aho P, Rossi PM, Isokangas E, Kløve B (2015) Fully integrated surface-subsurface flow modelling of groundwater-lake interaction in an esker aquifer: model verification with stable isotopes and airborne thermal imaging. J Hydrol 522:391–406

Ala-aho P, Tetzlaff D, McNamara JP, Laudon H, Soulsby C (2017) Using isotopes to constrain water flux and age estimates in snow-influenced catchments using the STARR (spatially distributed tracer-aided rainfall–runoff) model. Hydrol Earth Syst Sci 21: 5089–5110

Almasri MN, Kaluarachchi JJ (2007) Modeling nitrate contamination of groundwater in agricultural watersheds. J Hydrol 343:211–229

Ameli A, Amvrosiadi N, Grabs T, Laudon H, Creed I, McDonnell J, Bishop K (2016) Hillslope permeability architecture controls on subsurface transit time distribution and flow paths. J Hydrol 543: 17–30

Barthel R, Banzhaf S (2016) Groundwater and surface water interaction at the regional-scale: a review with focus on regional integrated models. Water Resour Manag 30:1–32. https://doi.org/10.1007/s11269-015-1163-z

Basu NB, Jindal P, Schilling KE, Wolter CF, Takle ES (2012) Evaluation of analytical and numerical approaches for the estimation of groundwater travel time distribution. J Hydrol 475:65–73. https://doi.org/10.1016/j.jhydrol.2012.08.052

Bathurst JC (1986) Sensitivity analysis of the system Hydrologique European for an upland catchment. J Hydrol 87(1-2):103–123. https://doi.org/10.1016/0022-1694(86)90117-4

Berg SJ, Sudicky EA (2019) Toward large-scale integrated surface and subsurface modeling. Groundwater 57(1):1–2. https://doi.org/10.1111/gwat.12844

Beven K (1989) Changing ideas in hydrology-the case of physically based models. J Hydrol 105(1-2):157–172. https://doi.org/10.1016/0022-1694(89)90101-7

Beven K, Davies J (2015) Velocities, celerities and the basin of attraction in catchment response. Hydrol Process 29:5214–5226. https://doi.org/10.1002/hyp.10699

Birkel C, Soulsby C (2015) Advancing tracer-aided rainfall-runoff modelling: a review of progress, problems and unrealised potential. Hydrol Process 29:5227–5240. https://doi.org/10.1002/hyp.10594

Birkel C, Soulsby C (2016) Linking tracers, water age and conceptual models to identify dominant runoff processes in a sparsely monitored humid tropical catchment: linking tracers, water age and conceptual models in the humid tropics. Hydrol Process 30:4477–4493. https://doi.org/10.1002/hyp.10941

Birkel C, Tetzlaff D, Dunn SM, Soulsby C (2010) Towards a simple dynamic process conceptualization on in rainfall-runoff models using multi-criteria calibration and tracers in temperate, upland catchments. Hydrol Process 24(3):260–275. https://doi.org/10.1002/hyp.7478

Birkel C, Tetzlaff D, Dunn SM, Soulsby C (2011) Using time domain and geographic source tracers to conceptualize streamflow generation processes in lumped rainfall-runoff models. Water Resour Res 47: W02515. https://doi.org/10.1029/2010WR009547

Birkel C, Duvert C, Correa A, Munksgaard NC, Maher DT, Hutley LB (2020) Tracer-aided modeling in the low-relief, wet-dry tropics suggests water ages and DOC export are driven by seasonal wetlands and deep groundwater. Water Resour Res 56(4):e2019WR026175. https://doi.org/10.1029/2019WR026175

Boubacar AB, Moussa K, Yalo N, Berg SJ, Erler AR, Hwang HT, Khader O (2020) Sudicky EA (2020) characterization of groundwater-surface water interactions using high resolution integrated 3D hydrological model in semiarid urban watershed of Niamey, Niger. J Afr Earth Sci 162:103739. https://doi.org/10.1016/j.jafrearsci.2019.103739

Brunner P, Simmons CT (2012) HydroGeoSphere: a fully integrated, physically based hydrological model. Groundwater 50:170–176. https://doi.org/10.1111/j.1745-6584.2011.00882.x

Chen J, Sudicky EA, Davison JH, Frey SK, Park YJ, Hwang HT, Erler AR, Berg SJ, Callaghan MV, Miller K, Ross M, Peltier WR (2019) Towards a climate driven simulation of coupled surface-subsurface hydrology at the continental scale: a Canadian example. Can Water Resour J. https://doi.org/10.1080/07011784.2019.1671235

Cordes C, Kinzelbach W (1992) Continuous groundwater velocity fields and path lines in linear, bilinear, and trilinear finite elements. Water Resour Res 28:2903–2911. https://doi.org/10.1029/92WR01686

Cornaton F, Perrochet P (2006) Groundwater age, life expectancy and transit time distributions: 1. generalized reservoir theory. Adv Water Resour 29:1267–1291. https://doi.org/10.1016/j.advwatres.2005.10.009

Davies J, Beven KJ, Nyberg L, Rodhe A (2011) A discrete particle representation of hillslope hydrology: hypothesis testing in reproducing a tracer experiment at Gårdsjon, Sweden. Hydrol Process 25:3602–3612. https://doi.org/10.1002/hyp.8085

Davies J, Beven KJ, Rodhe A, Nyberg L, Bishop K (2013) Integrated modelling of flow and residence times at the catchment scale with multiple interacting pathways. Water Resour Res 49(8):4738–4750. https://doi.org/10.1002/wrcr.20377

Davison JH, Hwang HT, Sudicky EA, Mallia DV, Lin JC (2018) Full coupling between the atmosphere, surface, and subsurface for integrated hydrologic simulation. J Adv Model 10:43–53. https://doi.org/10.1002/2017MS001052

Decker M (2015) Development and evaluation of a new soil moisture and runoff parameterization for the CABLE LSM including subgrid-scale processes. J Adv Model 7(4):1788–1809. https://doi.org/10.1002/2015MS000507

Dehaspe J, Birkel C, Tetzlaff D, Sánchez-Murillo R, Durán-Quesada AM, Soulsby C (2018) Spatially distributed tracer-aided modelling to explore water and isotope transport, storage and mixing in a pristine, humid tropical catchment. Hydrol Process 32:3206–3224. https://doi.org/10.1002/hyp.13258

Delavau CJ, Stadnyk T, Holmes T (2017) Examining the impacts of precipitation isotope input ($\delta^{18}O$) on distributed, tracer-aided hydrological modeling. Hydrol Earth Syst Sci 21:2595–2614. https://doi.org/10.5194/hess-21-2595-2017

Domenico PA, Palciauskas VV (1973) Theoretical analysis of forced convective heat transfer in regional ground-water flow. Geol Soc Am Bull 84(12):3803–3814. https://doi.org/10.1130/0016-76061973)84<3803:TAOFCH>2.0.CO;2

Dong L (2014) Analytical study to understand groundwater flow system and surface warming effect using subsurface thermal regimes- A case study in Kumamoto area, Japan. PhD Thesis, Dept. of Earth and Environmental Science, Kumamoto University, Japan

Dunn SM, Birkel C, Tetzlaff D, Soulsby C (2010) Transit time distributions of a conceptual model: their characteristics and sensitivities. Hydrol Process 24:1719–1729. https://doi.org/10.1002/hyp.7560

Erler AR, Frey SK, Khader O, d'Orgeville M, Park YJ, Hwang HT, Lapen DR, Peltier WR, Sudicky EA (2019) Simulating climate change impacts on surface water resources within a lake-affected region using regional climate projections. Water Resour Res 55: 130–155. https://doi.org/10.1029/2018WR024381

Fenicia F, Wrede S, Kavetski D, Pfister L, Savenije HHG, McDonnell JJ (2010) Assessing the impact of mixing assumptions on the estimation of streamwater mean residence time estimation. Hydrol Process 24(12):1730–1742. https://doi.org/10.1002/hyp.7595

Frei S, Lischeid G, Fleckenstein JH (2010) Effects of micro-topography on surface-subsurface exchange and runoff generation in a virtual riparian wetland: a modeling study. Adv Water Resour 33:1388–1401. https://doi.org/10.1016/j.advwatres.2010.07.006

Geological Survey of Japan, AIST (ed) (2009) Seamless digital geological map of Japan 1: 200,000. Research information database DB084. Geological Survey of Japan, National Institute of Advanced Industrial Science and Technology, Tokyo

Goderniaux P, Brouyvère S, Fowler HJ, Blenkinsop S, Therrien R, Orban P, Dassargues A (2009) Large scale surface-subsurface hydrological model to assess climate change impacts on groundwater reserves. J Hydrol 373:122–138. https://doi.org/10.1016/j.jhydrol.2009.04.017

Goode DJ (1996) Direct simulation of groundwater age. Water Resour Res 32(2):289–296. https://doi.org/10.1029/95WR03401

Hardy RJ, Bates PD, Anderson MG (1999) The importance of spatial resolution in hydraulic models for floodplain environments. J

Hydrol 216(1–2):124–136. https://doi.org/10.1016/S0022-1694(99)00002-5

Heidbuchel I, Troch PA, Lyon SW (2013) Separating physical and meteorological controls of variable transit times in zero-order catchments. Water Resour Res 49:7644–7657. https://doi.org/10.1002/2012WR013149

Hosono T, Tokunaga T, Kagabu M, Nakata H, Orishikida T, Lin IT, Shimada J (2013) The use of $\delta^{15}N$ and $\delta^{18}O$ tracers with an understanding of groundwater flow dynamics for evaluating the origins and attenuation mechanisms of nitrate pollution. Water Res 47:2661–2675. https://doi.org/10.1016/j.watres.2013.02.020

Hosono T, Tokunaga T, Tsushima A, Shimada J (2014) Combined use of $\delta^{13}C$, $\delta^{15}N$, and $\delta^{34}S$ tracers to study anaerobic bacterial processes in groundwater flow systems. Water Res 54:284–296. https://doi.org/10.1016/j.watres.2014.02.005

Hosono T, Yamada C, Shibata T, Tawara Y, Wang CY, Manga M, Rahman ATMS, Shimada J (2019) Coseismic groundwater drawdown along crustal ruptures during the 2016 mw 7.0 Kumamoto earthquake. Water Resour Res 55(7):5891–5903. https://doi.org/10.1029/2019WR024871

Hosono T, Hossain S, Shimada J (2020) Hydrobiogeochemical evolution along the regional groundwater flow systems in volcanic aquifers in Kumamoto, Japan. Env Earth Sci 79:410. https://doi.org/10.1007/s12665-020-09155-4

Hossain S, Hosono T, Ide K, Matsunaga M, Shimada J (2016a) Redox processes and occurrence of arsenic in a volcanic aquifer system of Kumamoto area, Japan. Environ Earth Sci 75(9):740. https://doi.org/10.1007/s12665-016-5557-x

Hossain S, Hosono T, Yang H, Shimada J (2016b) Geochemical processes controlling fluoride enrichment in groundwater at the western part of Kumamoto area, Japan. Water Air Soil Pollut 227(10):385. https://doi.org/10.1007/s11270-016-3089-3

Hrachowitz M, Savenije H, Bogaard TA, Tetzlaff D, Soulsby C (2013) What can flux tracking teach us about water age distribution patterns and their temporal dynamics? Hydrol Earth Syst Sci 17(2):533–564. https://doi.org/10.5194/hess-17-533-2013

Hwang HT, Park YJ, Sudicky EA, Berg SJ, McLaughlin R, Jones JP (2018) Understanding the water balance paradox in the Athabasca River basin, Canada. Hydrol Process. https://doi.org/10.1002/hyp,11449

Ichiyanagi K, Shimada J, Kagabu M, Saita S, Mori K (2012) Simulations of tritium age and $\delta^{18}O$ distributions in groundwater by using surface-subsurface coupling full-3D distribution model (GETFLOWS) in Kumamoto, Japan. In: 39th congress of the International Association of Hydrogeologists (IAH), Sheraton on the Falls Conference Centre, Niagara Falls, ON, Canada, September 2012

Ide K, Hosono T, Kagabu M, Fukamizu K, Tokunaga T, Shimada J (2020) Changes of groundwater flow systems after the 2016 mw 7.0 Kumamoto earthquake deduced by stable isotopic and CFC-12 compositions of natural springs. J Hydrol 583:124551. https://doi.org/10.1016/j.jhydrol.2020.124551

Itoh K, Tosaka H, Nakajima K, Nakagawa M (2000) Application of surface-subsurface flow coupled with numerical simulator to runoff analysis in an actual field. Hydrol Process 14:417–430. https://doi.org/10.1002/(SICI)1099-1085(20000228)14:3<417::AID-HYP946>3.0.CO;2-O

Ivanov VY, Vivoni ER, Bras RL, Entekhabi D (2004) Preserving high-resolution surface and rainfall data in operational scale basin hydrology: a fully-distributed physically-based approach. J Hydrol 298(1–4):80–111. https://doi.org/10.1016/j.jhydrol.2004.03.041

Japan Meteorological Agency (2020) https://www.jma.go.jp/jma/indexe.html. Accessed April 2020

Jing M, Heße F, Kumar R, Kolditz O, Attinger S (2018) Influence of input and parameter uncertainty on the prediction of catchment-scale groundwater travel time distributions. Hydrol Earth Syst Sci 23(1). https://doi.org/10.5194/hess-2018-383

Kagabu M, Matsunaga M, Ide K, Momoshima N, Shimada J (2017) Groundwater age determination using ^{85}Kr and multiple age tracers SF_6, CFCs and ^{3}H to elucidate regional groundwater flow systems. J Hydrol Reg Stud 12:165–180. https://doi.org/10.1016/j.ejrh.2017.05.003

Kim M, Pangle LA, Cardoso C, Lora M, Volkmann TH, Wang Y, Harman CJ, Troch PA (2016) Transit time distributions and storage selection functions in a sloping soil lysimeter with time-varying flow paths: direct observation of internal and external transport variability. Water Resour Res 52:7105–7129. https://doi.org/10.1002/2016WR018620

Kiriyama T, Ichikawa T (2004) Preservation of ground water basin recharging by paddy field. Ann J Hydraul Eng 48:373–378. https://doi.org/10.2208/prohe.48.373

Kitamura A, Kurikami H, Sakuma K, Malins A, Okumura M, Machida M, Mori K, Tada K, Tawara Y, Kobayashi T, Yoshida T, Tosaka H (2016) Redistribution and export of contaminated sediment within eastern Fukushima Prefecture due to typhoon flooding. Earth Surf Process Landf 41:1708–1726. https://doi.org/10.1002/esp.3944

Knighton J, Saia SM, Morris CK, Archiblad JA, Walter MT (2017) Ecohydrologic considerations for modeling of stable water isotopes in a small intermittent watershed. Hydrol Process 31:2438–2452. https://doi.org/10.1002/hyp.11194

Kollet SJ, Maxwell RM (2006) Integrated surface–groundwater flow modeling: a free-surface overland flow boundary condition in a parallel groundwater flow model. Adv Water Resour 29:945–958. https://doi.org/10.1016/j.advwatres.2005.08.006

Kollet SJ, Maxwell RM (2008) Demonstrating fractal scaling of baseflow residence time distributions using a fully-coupled groundwater and land surface model. Geophys Res Lett 35(7):L07402. https://doi.org/10.1029/2008GL033215

Kumamoto Prefecture and Kumamoto City (1986) General groundwater survey report of Kumamoto area (in Japanese). Kumamoto Prefecture and Kumamoto City, Japan, 90 pp

Kumamoto prefecture and Kumamoto city (1995) The Investigation Report on the Groundwater Protection and Management in Kumamoto Area, Kumamoto, Japan (in Japanese), Kumamoto prefecture and Kumamoto City, Japan, 122 pp

Kuppel S, Tetzlaff D, Maneta MP, Soulsby C (2018) EcH2O-iso 1.0: water isotopes and age tracking in a process-based, distributed ecohydrological model. Geosci Model Dev 11:3045–3069. https://doi.org/10.5194/gmd-11-3045-2018

Li Q, Unger AJA, Sudicky EA, Kassenaar D, Wexler EJ, Shikaze S (2008) Simulating the multi-seasonal response of a large-scale watershed with a 3D physically-based hydrologic model. J Hydrol 357:317–336. https://doi.org/10.1016/j.jhydrol.2008.05.024

Maples SR, Fogg GE (2019) Maxwell RM (2019) modeling managed aquifer recharge processes in a highly heterogeneous, semi-confined aquifer system. Hydrogeol J 27(8):2869–2888. https://doi.org/10.1007/s10040-019-02033-9

Matiatos I, Varouchakis EA, Papadopoulou MP (2019) Performance evaluation of multiple groundwater flow and nitrate mass transport numerical models. Environ Model Assess 24:659–675. https://doi.org/10.1007/s10666-019-9653-7

Maxwell RM, Condon LE, Kollet SJ, Maher K, Haggerty R, Forrester MM (2016) The imprint of climate and geology on the residence times of groundwater. Geophys Res Lett 43:701–708. https://doi.org/10.1002/2015GL066916

McCallum JL, Cook PG, Simmons CT (2015) Limitations of the use of environmental tracers to infer groundwater age. Groundwater 53:56–70. https://doi.org/10.1111/gwat.12237

McDonnell JJ, Beven K (2014) Debates on water resources: the future of hydrological sciences: a common path forward? A call to action aimed at understanding velocities, celerities and residence time

distributions of the headwater hydrograph. Water Resour Res 50: 5342–5350. https://doi.org/10.1002/2013WR015141

McGuire KJ, McDonnell JJ (2015) Preface: tracers advances in catchment hydrology. Hydrol Process 29:5135–5138. https://doi.org/10.1002/hyp.10740

Miles OW, Novakowski KS (2016) Large water-table response to rainfall in a shallow bedrock aquifer having minimal overburden cover. J Hydrol 541:1316–1328. https://doi.org/10.1016/j.jhydrol.2016.08.034

Miyakoshi A, Taniguchi M, Ide K, Kagabu M, Hosono T, Shimada J (2020) Identification of changes in subsurface temperature and groundwater flow after the 2016 Kumamoto earthquake using long-term well temperature–depth profiles. J Hydrol 582:124530. https://doi.org/10.1016/j.jhydrol.2019.124530

Miyamoto N, Shibasaki T, Takahashi H, Hatakeyama A, Yamamoto S (1962) Geology and groundwater of the western foot of Aso volcano- a study of confined groundwater of Japan. J Geol Soc Japan 68:282–292

Miyoshi M, Furukawa K, Shinmura T, Shimono M, Hasenaka T (2009) Petrography and whole-rock geochemistry of Pre-Aso lavas from the caldera wall of Aso volcano, central Kyushu. J Geol Soc Japan 115:672–687

MLIT (2020) Water information system. Ministry of Land, Infrastructure, Transport and Tourism of Japan. http://www1.river.go.jp/. Accessed April 2020

Momoshima N, Inoue F, Ohta T, Mahara Y, Shimada J, Ikawa R, Kagabu M, Ono M, Yamaguchi K, Sugihara S, Taniguchi M (2011) Application of ^{85}Kr dating to groundwater in volcanic aquifer of Kumamoto area, Japan. J Radioanal Nucl Chem 287:761–767. https://doi.org/10.1007/s10967-010-0821-0

Mori K, Tada K, Tawara Y, Ohno K, Asami M, Kosaka K, Tosaka H (2015) Integrated watershed modeling for simulation of spatio-temporal redistribution of post-fallout radionuclides: application in radiocesium fate and transport processes derived from the Fukushima accident. Environ Model Softw 72:126–146. https://doi.org/10.1016/j.envsoft.2015.06.012

Moriasi DN, Arnold JG, Van Liew MW, Bingner RL, Harmel RD, Veith TL (2007) Model evaluation guidelines for systematic quantification of accuracy in watershed simulations. Trans ASABE 50:885–900. https://doi.org/10.13031/2013.23153

Munz M, Oswald SE, Schmidt C (2017) Coupled long-term simulation of reach-scale water and heat fluxes across the river–groundwater interface for retrieving hyporheic residence times and temperature dynamics. Water Resour Res 53:8900–8924. https://doi.org/10.1002/2017WR020667

Nakayama H, Furusawa W, Hase Y, Aramaki S (2019) Geological cross-section maps in Kumamoto area –subsurface geology and the Kumamoto earthquake–. Research Association for Subsurface Geology of Kumamoto, Kumanichi Publisher, Kumamoto, pp 114 (in Japanese)

Nash JE, Sutcliffe JV (1970) River flow forecasting through conceptual models part I: a discussion of principles. J Hydrol 10:282–290. https://doi.org/10.1016/0022-1694(70)90255-6

Okumura A, Hosono T, Boateng D, Shimada J (2018) Evaluations of the downward velocity of soil water movement in the unsaturated zone in a groundwater recharge area using δ^{18}O tracer: the Kumamoto region, southern Japan. Geol Croat 71(2):65–82. https://doi.org/10.4154/gc.2018.09

Ono, K, Watanabe K (1985) Geological map of Aso volcano (1:50,000). In: Geological map of volcanoes 4 (in Japanese with English abstract). Geological Survey of Japan, Tokyo

Oshima I (2010) Administration for groundwater management in the Kumamoto area. J Groundw Hydrol 52:49–64

Peaceman DW (1983) Interpretation of well-block pressure in numerical reservoir simulation with non-square grid blocks and anisotropic permeability. Soc Pet Eng J:531–543. https://doi.org/10.2118/10528-PA

Piovano TI, Tetzlaff D, Carey SK, Shatilla NJ, Smith A, Soulsby C (2019) Spatially distributed tracer-aided runoff modelling and dynamics of storage and water ages in a permafrost-influenced catchment. Hydrol Earth Syst Sci 23:2507–2523. https://doi.org/10.5194/hess-23-2507-2019

Pruess K, Oldenburg C, Moridis G (1999) TOUGH2 user's guide, version 2.0. Report LBNL-43134, Lawrence Berkeley National Laboratory, Berkeley, CA

Rahman ATMS, Hosono T, Kisi O, Boateng D, Imon AHM (2020a) A minimalistic approach for evapotranspiration estimation using prophet model. Hydrol Sci J. https://doi.org/10.1080/02626667.2020.1787416

Rahman ATMS, Hosono T, Quilty JM, Das J, Basak A (2020b) Multiscale groundwater level forecasting: coupling new machine learning approaches with wavelet transforms. Adv Water Resour 141:103595. https://doi.org/10.1016/j.advwatres.2020.103595

Rassam DW, Peeters L, Pickett T, Jolly I, Holz L (2013) Accounting for surface-groundwater interactions and their uncertainty in river and groundwater models: a case study in the Namoi River, Australia. Environ Model Softw 50:108–119. https://doi.org/10.1016/j.envsoft.2013.09.004

Sakuma K, Kitamura A, Malins A, Kurikami H, Machida M, Mori K, Tada K, Kobayashi T, Tawara Y, Tosaka H (2017) Characteristics of radio-cesium transport and discharge between different basins near to the Fukushima Dai-ichi nuclear power plant after heavy rainfall events. J Environ Radioact 169–170:130–150. https://doi.org/10.1016/j.jenvrad.2016.12.006

Sakuma K, Malins A, Funaki H, Kurikami H, Niizato T, Nakanishi T, Mori K, Tada K, Kobayashi T, Kitamura A, Hosomi M (2018) Evaluation of sediment and 137Cs redistribution in the Oginosawa River catchment near the Fukushima Dai-ichi nuclear power plant using integrated watershed modeling. J Environ Radioact 182:44–51. https://doi.org/10.1016/j.jenvrad.2017.11.021

Samaniego L, Kumar R, Attinger S (2010) Multiscale parameter regionalization of a grid-based hydrologic model at the mesoscale. Water Resour Res 46:W05523. https://doi.org/10.1029/2008WR007327

Scheliga B, Tetzlaff D, Nuetzmann G, Soulsby C (2019) Assessing runoff generation in riparian wetlands: monitoring groundwater–surface water dynamics at the micro-catchment scale. Environ Monit Assess 191(2). https://doi.org/10.1007/s10661-019-7237-2

Schilling OS, Cook PG, Brunner P (2019) Beyond classical observations in hydrogeology: the advantages of including exchange flux, temperature, tracer concentration, residence time, and soil moisture observations in groundwater model calibration. Rev Geophys 57:146–182. https://doi.org/10.1029/2018RG000619

Shen C, Phanikumar MS (2010) A process-based, distributed hydrologic model based on a large-scale method for surface–subsurface coupling. Adv Water Resour 33:1524–1541. https://doi.org/10.1016/j.advwatres.2010.09.002

Shimada J (2012) Sustainable management of groundwater resources for 700,000-plus residents: a practical example of the transboundary management of groundwater resources in the Kumamoto area, Japan. In: Taniguchi M, Shiraiwa T (eds) The dilemma of boundaries: toward a new concept of catchment. Springer, Japan, pp 235–246. https://doi.org/10.1007/978-4-431-54035-9_20

Shimada J, Ichiyanagi K, Kagabu M, Saita S, Mori K (2012) Evaluation of long-term artificial groundwater recharge through leaky rice paddies with a 500 year history. In: 39th congress of the International Association of Hydrogeologists (IAH), Sheraton on the Falls Conference Centre, Niagara Falls, ON, Canada, September 2012

Shimano Y, Taniguchi M, Kayane I (1992) Characteristics of groundwater temperature in the upland areas at the western foot of Aso volcanoes. JAHS 19:155–169

Smith MB, Seo J, Koren VI, Reed SM, Zhang Z, Duan Q, Moreda F, Cong S (2004) The distributed model intercomparison project (DMIP): motivation and experiment design. J Hydrol 298:4–26. https://doi.org/10.1016/j.jhydrol.2004.03.040

Smith A, Welch C, Stadnyk T (2016) Assessment of a lumped coupled flow-isotope model in data scarce boreal catchments. Hydrol Process 30:3871–3884

Spanoudaki K, Stamou AI, Nanou-Giannarou A (2009) Development and verification of a 3-D integrated surface water-groundwater model. J Hydrol 375:410–427. https://doi.org/10.1016/j.jhydrol.2009.06.041

Stolp BJ, Solomon DK, Suckow A, Vitvar T, Rank D, Aggarwal PK, Han LF (2010) Age dating base flow at springs and gaining streams using helium-3 and tritium: Fischa-Dagnitz system, southern Vienna Basin, Austria. Water Resour Res 46(7):W07503. https://doi.org/10.1029/2009WR008006

Sudicky EA (2013) A physically-based modelling approach to assess the impact of climate change on Canadian surface and groundwater resources. In: 3rd International HydroGeoSphere User Conference 2013, Neuchatel, Switzerland, April 2013

Sutanudjaja EH, van Beek LPH, de Jong SM, van Gee FC, Bierkens MFP (2011) Large-scale groundwater modeling using global datasets: a test case for the Rhine-Meuse basin. Hydrol Earth Syst Sci 15:2913–2935

Takemori Y, Ichikawa T (2007) On effect of groundwater evaluation by keeping water in no use paddy field in the middle Shira-River area. Bull Sch Eng Kyushu Tokai Univ 34:1–8

Taniguchi M, Shimada J, Uemura T (2003) Transient effects of surface temperature and groundwater flow on subsurface temperature in Kumamoto plain, Japan. Phys Chem Earth 28:477–486. https://doi.org/10.1016/S1474-7065(03)00067-6

Taniguchi M, Burnett K, Shimada J, Hosono T, Wada CA, Ide K (2019) Recovery of lost nexus synergy via payment for environmental services in Kumamoto, Japan. Front Environ Sci 7:1–8. https://doi.org/10.3389/fenvs.2019.00028

Tawara Y, Hosono T, Fukuoka Y, Yoshida T, Shimada J (2020) Quantitative assessment of the changes in regional water flow systems caused by the 2016 Kumamoto earthquake using numerical modeling. J Hydrol 583:124559. https://doi.org/10.1016/j.jhydrol.2020.124559

Therrien R, McLaren RG, Sudicky EA, Panday SM (2010) HydroGeoSphere: a three-dimensional numerical model describing fully-integrated subsurface and surface flow and solute transport. Groundwater Simulations Group, DRAFT-2010, Canada. https://www.ggl.ulaval.ca/fileadmin/ggl/documents/rtherrien/hydrogeosphere.pdf

Thornthwaite CW (1948) An approach toward a rational classification of climate. Geogr Rev 38(1):55–94. https://doi.org/10.2307/210739

Thunvik R (1987) Calculations on HYDROCOIN level 2, case 1 using the GWHRT flow model (no. SKB-TR-87-04). Swedish Nuclear Fuel and Waste Management, Stockholm

Tosaka H (2007) Mathematics of hydrological cycle in Geosphere. University Tokyo Press, pp 342

Tosaka H, Kojima K, Miki A, Chino T (1996) Numerical simulation of surface-subsurface-coupled, 2-phase, 3-dimensional fluid behavior. J Japan Assoc Groundwater Hydrol 38:253–267

Tosaka H, Itoh K, Furuno T (2000) Fully coupled formulation of surface flow with 2-phase subsurface flow for hydrological simulation. Hydrol Process 14(3):449–464

Tosaka H, Mori K, Tada K, Tawara Y, Yamashita K (2010) A general-purpose terrestrial fluids/heat flow simulator for watershed system management. In: Proceedings of IAHR International Groundwater Symposium 2010, Valencia, Spain, September 2010

Tsuboyama Y, Sidle RC, Noguchi S, Hosoda I (1994) Flow and solute transport through the soil matrix and macropores of a hillslope segment. Water Resour Res 30(4):879–890. https://doi.org/10.1029/93WR03245

Van Huijgevoort MHJ, Tetzlaff D, Sutanudjaja EH, Soulsby C (2016a) Using high resolution tracer data to constrain water storage, flux and age estimates in a spatially distributed rainfall-runoff model. Hydrol Process 30(25):4761–4778

Van Huijgevoort M, Tetzlaff D, Sutanudjaja EH, Soulsby C (2016b) Visualisation of spatial patterns of connectivity and runoff ages derived from a tracer-aided model. Hydrol Process 25:4893–4895

VanderKwaak, JE (1999) Numerical simulation of flow and chemical transport in integrated surface–subsurface hydrologic system. PhD Thesis, University of Waterloo, Waterloo, ON, Canada

VanderKwaak JE, Loague K (2001) Hydrologic-response simulations for the R-5 catchment with a comprehensive physics-based model. Water Resour Res 37:999–1013. https://doi.org/10.1029/2000WR900272

Varni M, Carrera J (1998) Simulation of groundwater age distributions. Water Resour Res 34:3271–3281. https://doi.org/10.1029/98WR02536

Water Resources Development Study Group (1975) Groundwater survey report of Kumamoto area. Department of Geography, Education, Tokyo University, Tokyo

Weill S, Altissimo M, Cassiani G, Deiana R, Marani M, Putti M (2013) Saturated area dynamics and streamflow generation from coupled surface–subsurface simulations and field observations. Adv Water Resour 59:196–208. https://doi.org/10.1016/j.advwatres.2013.06.007

Weissmann GS, Zhang Y, LaBolle EM, Fogg GE (2002) Dispersion of groundwater age in an alluvial aquifer system. Water Resour Res 38(10):1198. https://doi.org/10.1029/2001WR000907

Wilusz DC, Harman CJ, Ball WB, Maxwell RM, Buda AR (2020) Using particle tracking to understand flow paths, age distributions, and the paradoxical origins of the inverse storage effect in an experimental catchment. Water Resour Res. https://doi.org/10.1029/2019WR025140

Yamaguchi K (2010) Evaluation of groundwater residence time of Kumamoto area by using environmental tritium. BA Thesis, Department of Earth and Environmental Science, Kumamoto University, Japan

Zeng X, Hosono T, Ohta H, Niidome T, Shimada J, Morimura S (2016) Comparison of microbial communities inside and outside of a denitrification hotspot in confined groundwater. Int Biodeterior Biodegrad 114:104–109. https://doi.org/10.1016/j.ibiod.2016.05.019

Zhang H, Li Z, Saifullah M, Li Q, Li X (2016) Impact of DEM resolution and spatial scale: analysis of influence factors and parameters on physically based distributed model. Adv Meteorol. https://doi.org/10.1155/2016/8582041

Zhang Y, Weissmann G, Fogg G, Lu B, Sun H, Zheng C (2018) Assessment of groundwater susceptibility to non-point source contaminants using three-dimensional transient indexes. Int J Environ Res Public Health 15(6):1177. https://doi.org/10.3390/ijerph15061177